ACS Sustainable Chemistry & Engineering

pubs.acs.org/journal/ascecg

Research Article

Hybrid Computationally Guided Strategies for Engineering a Laminaribiose Phosphorylase to Facilitate the Industrial Production of Laminaribiose *In Vitro*

Shangshang Sun, Qiangzi Li, Lin Fan, Yi-Heng P. Job Zhang, and Chun You*

Cite This: https://doi.org/10.1021/acssuschemeng.3c06089

Read Online

ACCESS | Metrics & More | Article Recommendations | Supporting Information

ABSTRACT: Efficient enzymatic synthetic pathways for biomanufacturing chemicals often require addressing bottlenecks by enhancing the catalytic efficiency or thermostability of unsatisfied enzymes. Laminaribiose, a valuable commodity disaccharide, can be biosynthesized from starch *via* an *in vitro* four-enzyme cascade previously described, but a thermolabile laminaribiose phosphorylase from *Paenibacillus* sp. YM1 (PsLBP) is a potential bottleneck. Here, through several computationally guided approaches, the thermostability of PsLBP was successfully enhanced, with the best mutant, M8, exhibiting a 15.3 °C higher T_m value, a 71.1-fold longer half-life, and a 2.4-fold increased specific activity at 60 °C than those of the wild-type enzyme. Structure analysis and molecular dynamics simulations revealed that the formation of new disulfide bonds and salt bridges and the changes to hydrogen bonds optimized the overall structure and improved the thermostability of M8. Subsequently, by employing an industrial procedure of heat-permeabilized whole cells, the *in vitro* biosystem incorporating PsLBP-M8 in a volume of 30 L converted 100.0 g/L starch to ∼77.0 g/L laminaribiose with a molar yield of ∼75% at 60 °C. These findings highlight the utility of hybrid computationally guided strategies for engineering large proteins such as laminaribiose phosphorylase and demonstrate the power of adapting incompatible enzymes in *in vitro* biosystems to enhance industrial performance.

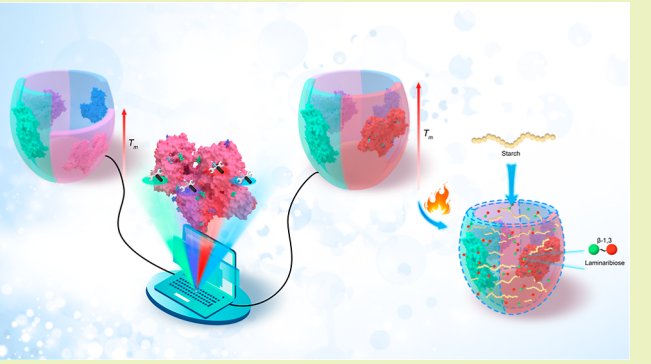

KEYWORDS: *computationally guided engineering, laminaribiose phosphorylase, thermostability, in vitro laminaribiose production system*

INTRODUCTION

Laminaribiose is a linear β (1,3)-linked disaccharide found in restricted quantities in natural sources, but it is present as subunits of natural polysaccharides, such as seaweed laminarin, pachyman, and lichenin.[1] Recently, β-1,3 glucans from white button mushrooms (2022) and *Euglena gracilis* (2014) were approved as "generally recognized as safe" by the U.S. Food and Drug Administration, and both Curdlan[2] and lentinan[3] have been reported to exhibit intestinal anti-inflammatory activity in mice. Compared with these β-1,3 glucans, laminaribiose has additional value for its illustrious functional roles, including as a preservative,[4] as a powerful seed germination agent widely employed in the sphere of agriculture,[5] as precursors for building blocks to provide hyaluronic acid within the pharmaceutical trade,[6] and as a very important prebiotic for increasing the number of bifidobacteria and lactobacilli.[7] Currently, most of the laminaribiose is produced through partial enzymatic or acid hydrolysis of natural β-1,3 glucans.[8,9] However, the composition of the resulting hydrolysate is complex, and the isolation of laminaribiose from such hydrolysates incurs high separation costs.[10] The chemical method for producing laminaribiose from glucose is another method for laminaribiose production; however, the chemical method process is troublesome to manage and suffers from laborious protection of group manipulations, harsh reaction conditions, cumbersome purification operations, and low overall yield.[11]

The biosynthesis of laminaribiose from glucose by β-glucosidase or from glucose and glucose 1-phosphate (G1P) by laminaribiose phosphorylase (LBP, EC 2.4.1.30)[12] has recently received increasing attention due to the readily accessible substrate, mild reaction conditions, environment-friendly process, and excellent regio- and stereoselectivity.[13] The synthesis of laminaribiose by glycosidases has several benefits that embody simplicity, accessibility, and easy operations, although the broad substrate specificity of β-

Received: September 21, 2023
Revised: February 7, 2024
Accepted: February 8, 2024

glucosidase synthesizes three main products (laminaribiose, sophorose, and cellobiose).[14,15] In contrast, LBP, which catalyzes ATP-independent phosphorolysis reactions with strict regioselectivity, is the ideal enzyme for the transformation of readily accessible saccharides to laminaribiose.[16−18] Many studies have investigated the use of sucrose or maltodextrin as a provider of G1P catalyzed by sucrose phosphorylase (SP) or α-glucan phosphorylase (αGP).[19] Muller *et al.*[20] reported the production of laminaribiose from sucrose and glucose catalyzed by SP and LBP, in which the reaction was carried out at 35 °C with a final yield of 55%. This low carbon conversion was attributed to the use of SP on sucrose to generate G1P, which is accompanied by 6-carbon fructose waste. Furthermore, an *in vitro* synthetic enzymatic biosystem containing αGP, α-glucosidase (αG), and LBP was constructed by our group to produce laminaribiose from maltodextrin at 50 °C, resulting in a product yield of 81.1%.[1,21,22] Notably, this enzymatic ensemble maximally utilized all glucose units present in the substrate (maltodextrin), thereby resulting in a much better atom efficiency in the synthesis process.

Carbohydrate conversion in the industry is preferably performed at elevated temperatures to prevent microbial contamination and to avoid excessive viscosity.[23] The *in vitro* biosynthesis reaction described above for laminaribiose production from maltodextrin can instead be performed with whole cells for industrialization, thus omitting certain preparatory steps, such as purification and separation of enzymes, and improving enzyme stability because of the macromolecular crowding in the cellular environment.[24] To increase the product yield and reaction rate in whole-cell biotransformations, it is important to take the cell membrane permeability into account, which affects the mass transfer. Heat treatment can be used to increase the permeabilization of cells, but this requires that all the enzymes of the *in vitro* biosystems are stable enough to survive after such treatment. In the *in vitro* laminaribiose production biosystem previously described, the αGP and αG are hyperthermophylic enzymes with optimal temperatures over 70 °C, but wild-type (WT) LBPs cannot satisfy this requirement of industrial applications. To date, only four enzymes have been reported to demonstrate phosphorolysis or synthesis activity of β-1,3-glycosidic bonds,[25−27] *E. gracilis* (EgLBP),[28,29] *Astasia ocellate* (AoLBP),[30] *Acholeplasma laidlawii* (AlLBP),[16] and *Paenibacillus* sp. (PsLBP).[12] Among them, EgLBP, AoLBP, and AlLBP are all medium-temperature enzymes with an optimal temperature of 30−40 °C; and PsLBP has an optimal temperature of 55 °C with a half-life ($t_{1/2}$) at 50 °C of 5.1 h, and it was used in our previous study of laminaribiose.[1,21,22] However, this enzyme loses its activity rapidly at the industrially relevant temperature of 60 °C.[1] The poor thermostability of PsLBP limits its application for producing laminaribiose at an industrial scale. Therefore, it is necessary to apply protein engineering methods to construct a more thermostable LBP for enhancing its industrial performance.

Protein engineering methods usually include two distinctive approaches: rational design and directed evolution.[31,32] Directed evolution based on random mutagenesis is an effective way to evolve targeted biocatalysts with a desired performance without depending on the knowledge of the three-dimensional structure of proteins, requiring high-throughput screening or effective selection strategies.[33] However, this method has low efficiency when engineering a protein with a high molecular weight,[34,35] and LBPs are large proteins in the form of a dimer, with monomer lengths ranging from 830 to 1111 amino acids. In contrast, rational protein design is generally less labor-intensive but demands a broad understanding of protein structure and function.[36] Recent decades have witnessed considerable efforts to improve protein stability through diverse rational strategies, including introducing hydrogen bonds, salt bridges, or disulfide bonds; improving core packing; optimizing surface charges; and increasing rigidity by mutating preferred residues.[37,38] These mutation sites can be predicted by computational approaches, including energy-based methods, phylogeny-based methods, machine learning, and hybrid methods.[39,40] The accuracy of the positive mutation sites that relies on individual algorithms suffers from a series of problems, such as insufficient conformational sampling, imbalances in the force fields, or intrinsic problems with existing data sets. Hybrid methods, including FRESCO,[41] FireProt,[42] PROSS,[43] and GRAPE,[44] incorporate several different complementary approaches to alleviate sampling bias.[40] For example, Damborsky *et al.* employed the FireProt strategy to improve the thermostability of two enzymes, DhaA and LinA, and achieved a significant increase in melting temperatures (T_m) of 24 and 21 °C, respectively.[42] Wu *et al.* developed the GRAPE strategy to improve the T_m of a PETase from *Ideonella sakaiensis* by 31 °C.[44] Thus, because the crystal structure of PsLBP is available, it is more appropriate to use rational design methods for engineering this large-sized enzyme.

In this study, a hybrid method that incorporated several different computationally guided approaches to predict the mutation sites was applied to stabilize PsLBP by introducing salt bridges and disulfide linkages, modifying unfavorable surface charge-bearing amino acids, and filling structure cavities. These mutation sites were scored based on the results of multifaceted computations mentioned above, then screened for chemically unreasonable mutated amino acids, and finally experimentally validated. After combining mutations, the best performing mutant PsLBP-M8 exhibited a longer half-life and higher T_m value than did PsLBP-WT, and the activity of PsLBP-M8 at 60 °C was much higher than that of PsLBP-WT. Molecular dynamics (MD) simulation and structure analysis were used to understand how these mutations improved the thermostability of PsLBP-M8. By employing the whole cells permeabilized by heat treatment, the *in vitro* biosystem containing M8 converted 100.0 g/L starch to ∼77.0 g/L laminaribiose with a molar yield of 75.0% at 60 °C in a volume of 30 L. This study not only provided insights into improving enzyme stability using a hybrid method but also laid a solid foundation for the industrial enzymatic production of laminaribiose from starch.

METHODS AND MATERIALS

Chemicals and Strains. All chemicals were of reagent grade and were purchased from Sigma-Aldrich (St. Louis, MO, USA) or Sinopharm (Shanghai, China) unless otherwise noted. The PCR enzyme used was Phusion high-fidelity DNA polymerase from New England Biolabs (Ipswich, MA, USA). The synthesis of the oligonucleotide primers and the DNA sequencing was performed at Genewiz (Suzhou, China). *Escherichia coli* DH5α was used for plasmid construction, and *E. coli* BL21 (DE3) was used for protein expression.

Plasmid Construction and Site-Directed Mutagenesis. The WT plasmid pET28a-pslbp encoding LBP from *Paenibacillus* sp. YM1 was obtained from our previous studies. Site-directed mutagenesis was

https://doi.org/10.1021/acssuschemeng.3c06089
ACS Sustainable Chem. Eng. XXXX, XXX, XXX−XXX

performed with the WT LBP plasmid as a template. In the present research, the LBP mutants were constructed with a pair of primers containing the corresponding codon at specified sites using a modified site-directed mutagenesis procedure (the primers utilized for the construction of the final positive mutants are listed in Table S1). Each reaction (50 μL) contained 100 pg of template plasmid pET28a-pslbp and 25 pmol of each mutagenic primer. The primers were phosphorylated with T4 Polynucleotide Kinase (New England Biolabs, Ipswich, MA, USA) at the 5′ end. The PCR products were incubated with DpnI (New England Biolabs, Ipswich, MA, USA) to digest the original DNA template, followed by the self-ligation by the NEB quick ligase kit (New England Biolabs, Ipswich, MA, USA), and the ligation product was transformed into *E. coli* TOP10. The introduced mutations were confirmed by sequencing.

***In Silico* Analysis.** In order to get stable variants, several strategies were applied to predict the potential mutation sites. EVCoupling was used to generate sequence alignments, calculate and evaluate of evolutionary couplings (ECs), and de novo predict structure and mutation effects.[45,46] The ECs harboring positively and/or negatively charged amino acid residues may make chance to form new salt-bridges. Based on the crystal structure of PsLBP (PDB ID: 6GGY), the Gibbs free energy changes (ΔG) of the wild type and mutants, which were from the virtual site-saturation mutagenesis, were calculated with FoldX.[39,47,48] Disulfide by Design 2 (DbD2, http://cp tweb.cpt.wayne.edu/DbD2/) was used to recognize the cysteine pairs, which are in the proper orientation to form a disulfide bond.[49] DbD2 provided comprehensive data encompassing three key aspects. First, it offered insights into the χ_3 torsion angle, which signifies the rotational movement of the two C_β atoms along the $S_\gamma-S_\gamma$ bond. Notably, the recorded observations indicated that the χ_3 angle exhibited notable peaks at −87 and +97°. Second, the data set presented valuable information regarding the energy variations involved in stabilizing and destabilizing disulfide bonds, commonly referred to as disulfide bond energy. Additionally, for each potential disulfide, the sum *B*-factor is calculated for each pair by summing the *B*-factor values of two residues, each representing the average *B*-factor of the backbone and β-carbon atoms, and a threshold of 40 is applied to select only those sum *B*-factor values that exceed this cutoff. An enzyme thermal stability system (ETSS) was developed using a suite of enzyme redesign algorithms to calculate the total interaction energy (E_{ij}) of each surface charged amino acid in PsLBP. The ETSS calculation is based on the Tanford−Kirkwood[50] model, which evaluates the contribution of a single charged residue to the overall stability, and incorporates factors such as solvent accessibility,[51] Gibbs free energy,[52] and electrostatic interactions[53] for further improvement. A negative E_{ij} value indicates a favorable interaction, while a positive E_{ij} value indicates an unfavorable one.[54,55] Therefore, the mutations on the residues with positive E_{ij} values may enhance the enzyme thermostability. The average root-mean-square fluctuation (RMSF) values for residues were calculated using Gromacs[56] and the B-Factor values of WT PsLBP (PDB ID: 6GGY) were extracted from the PDB structure file and calculated using the B-FITTER software.[57] Because PsLBP is a homodimer, the B-Factor of each residue was calculated by averaging the *B*-factor values of the same residue from chain A and chain B. Rosetta VIP (void identification and packing) Online Server (https://rosie.graylab.jhu.Edu/vip) was used to search for the hydrophobic void in proteins, determine the composition of amino acids around the voids, and mutate these amino acids into larger or nonpolar amino acids with side chain groups, aiming at improving the compactness of the enzyme package and the thermal stability of the enzyme.[39] The VIP energy change (ΔE) is formed by weighted combination of the Lennard-Jones attractive energy, Gaussian overlap energy, and hydrophobic surface area energy terms in Rosetta. This program initially identified several candidate mutants with negative $\Delta\Delta E$ (the change of ΔE value between the mutant and wild type, the smaller the $\Delta\Delta E$ value, the more stable the designed mutants) values. After each iteration, Rosetta VIP will provide a mutant with a specific amino acid for a specific mutation site that was predicted with the lowest $\Delta\Delta E$ value. The above process iterated until the mutation site with a lower $\Delta\Delta E$ value cannot be found; this simulation selects up to 5 rounds of iteration. The three-dimensional modeled structures of PsLBP variants were predicted by AlphaFold 2.[58,59] The program ClustalW from BioEdit (Carlsbad, CA, USA) was used to align 3 functionally characterized LBP sequences. PyMOL was used to visualize and analyze the modeled structures.

Overexpression and Purification of Recombinant Proteins. For the preparation of the recombinant proteins, *E. coli* BL21 (DE3) was transformed with each of the recombinant plasmids (pET28a-pslbp WT and mutants) to express recombinant LBP enzymes. The transformed cells were incubated at 37 °C in 1 L Erlenmeyer flasks containing 200 mL of LB medium with 50 μg/mL kanamycin or 100 μg/mL ampicillin with a rotary shaking rate of 250 rpm. When the OD_{600} reached 0.6−0.8, recombinant protein expression was induced by the addition of isopropyl-β-D-thiogalactopyranoside to a final concentration of 0.1 mM. The bacterial culture was then incubated at 16 °C for 18 h. The cells were harvested by centrifugation at 4 °C, washed twice with 50 mM phosphate buffer ($KH_2PO_4-K_2HPO_4$, pH 7.0), and resuspended in 20 mM HEPES buffer (pH 7.0) containing 50 mM NaCl. The cell pellets were lysed using a Fisher Scientific Sonic Dismembrator Model 500 (5 s pulse on and off, total 360 s, 20% amplitude) in an ice bath. After centrifugation at 4 °C and 8000*g* for 20 min, the enzymes underwent purification utilizing Ni-NTA resin with a 50 mM HEPES buffer (pH 7.0) supplemented with 50 mM NaCl and varying concentrations of imidazole. The protein concentrations subsequent to ultrafiltration were determined using the Bradford method with bovine serum albumin as the standard.

Determination of Kinetic Parameters and Enzyme Thermostability. The enzymatic activity for laminaribiose production, as well as the kinetic analysis for both reaction directions catalyzed by PsLBP-WT and its mutants, was carried out employing the methodology previously outlined.[1,21] All the assays were performed in 50 mM HEPES buffer (pH 7.0) with 5 mM $MgCl_2$ at 50 °C, and various kinetic parameters, such as k_{cat} and K_m, were calculated based on the Michaelis−Menten kinetic equation. As reported in the literature and supported by our preliminary investigations, the addition of $MgCl_2$ does not alter the characterization of the WT PsLBP. Furthermore, PsLBP does not inherently necessitate metal ions as activators; rather, $MgCl_2$ is introduced because of its role as an activator for αGP within the reaction system. One unit of enzyme activity was defined as the amount of enzyme or whole cells that generated 1 μmol of product per minute.

The thermostability was estimated by the ratio of the residual activity to the initial activity of the enzyme. Samples were diluted in 50 mM buffer (pH 7.0) with 5 mM $MgCl_2$ to a protein concentration of 1 mg/mL followed by incubating at 60, 65, and 70 °C, respectively. After the incubation, samples were chilled on ice immediately. Then, the residual activity was assayed at 50 °C as described above. The relationship between the natural logarithm of the residual activity and the inactivation time can be expressed as follows: ln (residual activity) = $-k_i t$, where k_i represents the inactivation rate and t denotes the inactivation time. Subsequently, the half-life ($t_{1/2}$) can be determined based on k_i using the formula: $t_{1/2} = \ln(2)/k_i$. All assays for enzyme thermostability determination were performed at least in triplicate.

Determination of Melting Temperature (T_m). The T_m values of PsLBP-WT and its variants were determined using differential scanning calorimetry (Nano DSC III, TA Instruments, New Castle, DE). The purified WT enzyme and mutants were diluted to a final concentration of 0.5 mg/mL. Baseline scans were repeated 5 times using the buffer same as that for enzyme purification and preservation. The operating parameters were set as follows: scanning temperature range: baseline and sample scan 20−100 °C; pressure: 3 atm; heating rate: 1 °C/min. Buffer baseline-corrected DSC data were used to fit the two-state scaled model to obtain the T_m values of the WT enzyme and mutants by TA Instruments NanoAnalyze software. All assays for enzyme thermostability determination were performed at least in duplicate.

Thiol Titration. The free thiol content was determined by reacting the purified enzymes with dithionitrobenzoic acid (DTNB).[60] Initially, a denaturing solution was prepared by combining 0.1 M sodium phosphate (pH 8.0) with 6 M guanidine hydrochloride

https://doi.org/10.1021/acssuschemeng.3c06089
ACS Sustainable Chem. Eng. XXXX, XXX, XXX−XXX

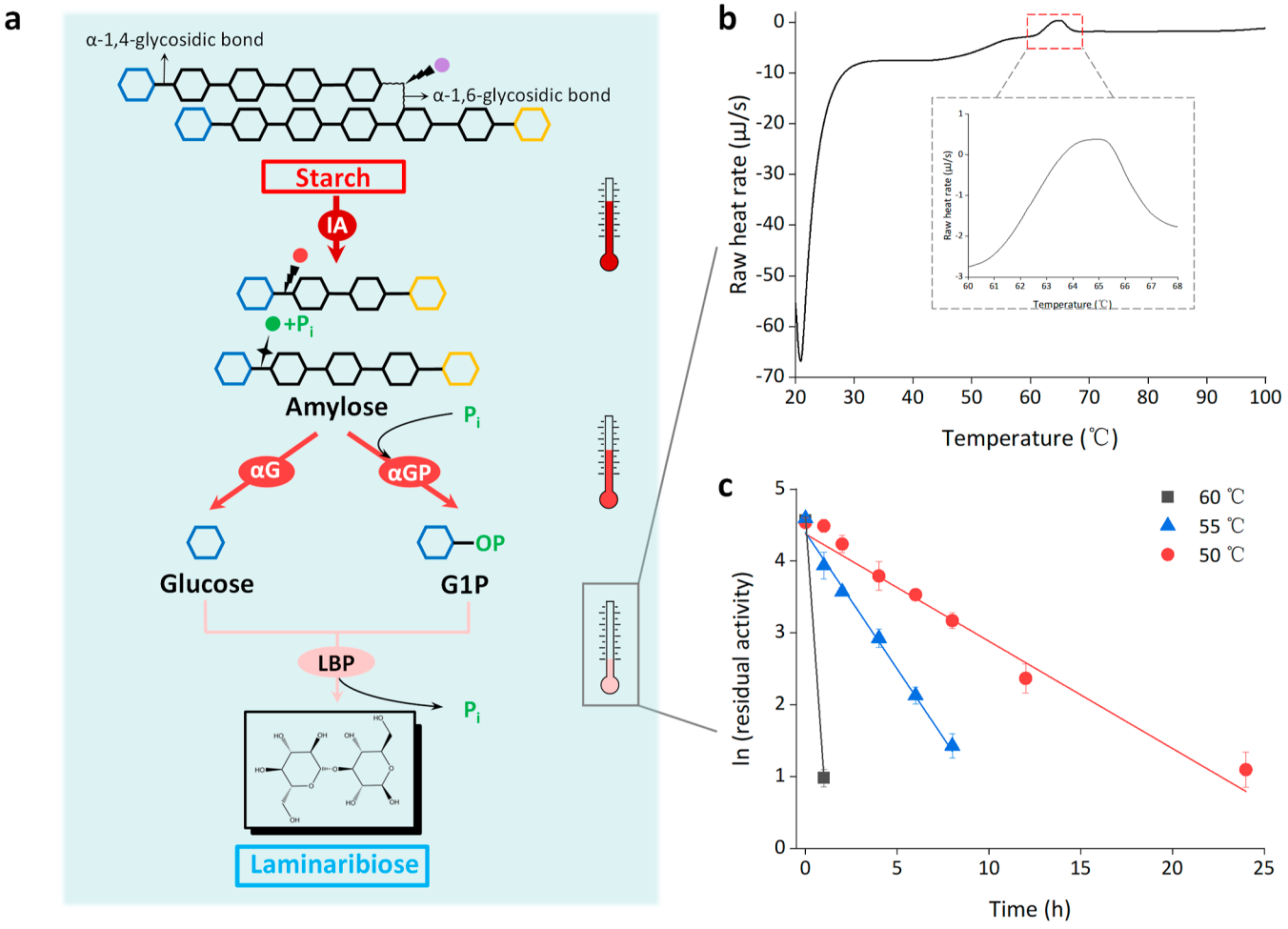

Figure 1. (a) *In vitro* synthetic enzymatic biosystem for laminaribiose production from starch. The enzymes are abbreviated as follows: isoamylase (IA), α-glucan phosphorylase (αGP), α-glucosidase (αG), and laminaribiose phosphorylase (LBP). The chemicals are abbreviated as follows: glucose-1-phosphate (G1P), inorganic phosphate (Pi). (b) DSC scan curves of PsLBP WT. (c) Half-lives determination of PsLBP WT at 50 (square), 55 (circle), and 60 °C (triangle). All data are averages of three independent experiments with standard deviations.

(GuHCl). Next, 3 mL of the denaturing solution was thoroughly mixed with the enzyme to ensure complete denaturation. Subsequently, 100 μL of 10 mM DTNB was added and thoroughly mixed. The absorbance at 412 nm was measured when no further color change was observed, with a control sample lacking the enzyme used for zero calibration. To facilitate reduction, the denatured protein was then treated with 25 mM dithiothreitol (DTT) and subsequently subjected to dialysis to remove DTT.[61] Thiol titration was performed by the addition of DTNB. The increase in thiols before and after DTT treatment indicated the formation of disulfide bonds.

Molecular Dynamics Simulations. The MD simulation was performed using GROMACS 2019.6[56] using the amber14sb as force field. The initial structure was solvated with a simple point-charge model of TIP3P water in a cubic simulation box (the layer of water at least 12.0 Å from the protein surface). Sufficient Na^+ was added to neutralize the negative charges in the system. The system was then subjected to a steepest descent energy minimization (50,000 steps) to give the maximum force below 1000 kJ/mol. Both of the maximum distances for Coulomb force and van der Waals radius were set at 14 Å.[62] The Particle Mesh Ewald method was used to calculate long-range electrostatic forces, and the maximum distance is set to 12 Å. Finally, a 100 ns MD simulation was performed on the whole system at 300 and 333 K, respectively. All bond lengths were constrained using the linear constraint solver (LINCS) algorithm,[63] and the time step of the simulation was set to 2 fs. The root means square deviation (rmsd) and the RMSF, which are important indexes for evaluating the protein structure, were calculated using GROMACS rms and RMSF tools. The time-dependent secondary structure was calculated using the do_dssp tool. Solvent-accessible surface area (SASA) was calculated using tools within the GROMACS sasa package. The total number of hydrogen bonds present in the crystal structure was calculated using a geometrical criterion according to which the cutoff distance between the donor and acceptor was less than 3.4 Å and the angle between the donor−hydrogen−acceptor was less than 30° for the H-bond to be present. The maximum distance for nonbond interaction was set to 10 Å. Postprocessing and analysis were performed using standard GROMACS tools and Visual MD.

Permeabilized Whole-Cell Bioconversion of Starch into Laminaribiose. For preparing permeabilized whole cells, cells were harvested from the culture broth (OD_{600} ~ 3) by centrifugation at 6000*g* for 6 min at room temperature and washed twice with 0.9% sodium chloride solution. Then, the washed cells were resuspended and proportionally concentrated in 50 mm HEPES buffer (pH 7.0) to the final OD_{600} of 100 (*i.e.*, a 100 mL culture broth with an initial OD_{600} of 3 was concentrated, resulting in 3 mL of resuspended material with a final OD_{600} of 100). The cell suspension was incubated at different temperatures from 50 to 70 °C for 20 min to obtain permeabilized whole cells. The whole-cell catalytic reactions for laminaribiose production were performed at 60 °C for 12 h in 50 mm HEPES buffer (pH 7.0) containing 100 g/L IA-treated maltodextrin and 10 mM phosphate (KH_2PO_4–K_2HPO_4, pH 7.0). The whole-cell amounts of *E. coli*/pET28a-TmαGP, *E. coli*/pET28a-BsαG, and *E. coli*/pET28a-PsLBP-WT or *E. coli*/pET28a-PsLBP-M8 to be added to the reaction systems were determined by the mathematical model

https://doi.org/10.1021/acssuschemeng.3c06089
ACS Sustainable Chem. Eng. XXXX, XXX, XXX−XXX

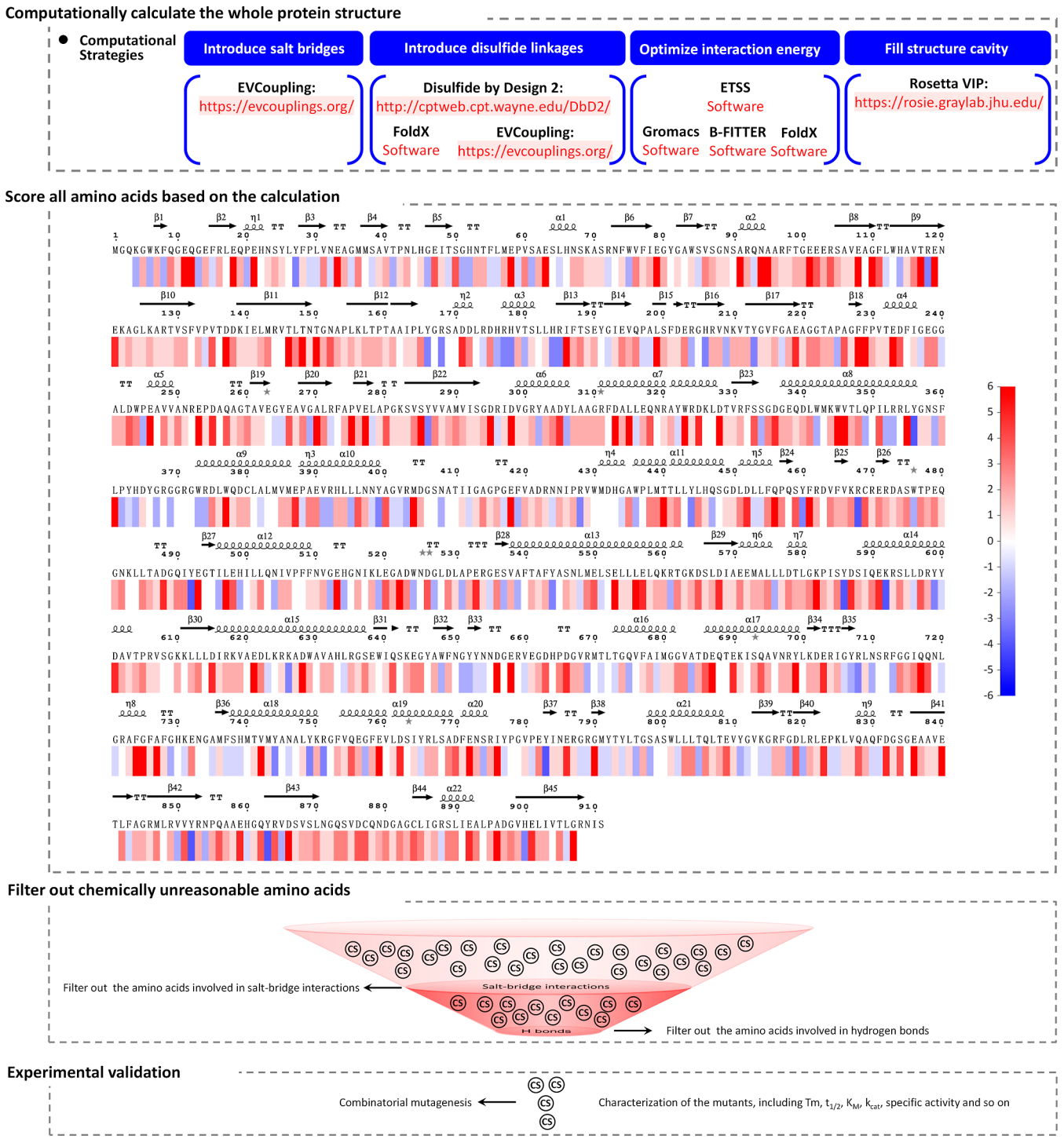

Figure 2. Schematic representation of the combined computer-aided rational design strategy. In step 1, the whole protein structure was calculated with multiple strategies to predict the mutation sites. In step 2, all mutations were scored based on the calculations of step 1. In step 3, the mutation sites with typical known pitfalls were eliminated. Then, the remaining designed mutation sites were selected for experimental validation.

presented in our previous study[21] as well as the expression levels of each enzyme. Samples were taken at different time intervals, and the laminaribiose content was determined by HPLC analysis as described previously.[1,21] All experiments were performed in triplicate.

RESULTS

A cost-effective *in vitro* enzymatic pathway with four enzymes for producing laminaribiose from starch was developed in our previous study (Figure 1a). The biosystem consisted of four enzymes that catalyzed the following reactions: first, isoamylase (IA) hydrolyzed α-1,6-glycosidic linkages of starch to produce amylose; second, alpha-glucan phosphorylase (αGP) phosphorylated amylose from the nonreducing ends to generate α-G1P in the presence of inorganic phosphate (P_i); meanwhile, alpha-glucosidase (αG) also hydrolyzed amylose from the nonreducing ends to yield glucose; finally, LBP catalyzed the synthesis of laminaribiose from G1P and glucose as substrates, releasing P_i. The released phosphate was recycled to maintain

https://doi.org/10.1021/acssuschemeng.3c06089
ACS Sustainable Chem. Eng. XXXX, XXX, XXX−XXX

constant pH and phosphate levels. We reported final product yields of laminaribiose obtained from 100 g/L starch that were higher than 80%, indicating that our *in vitro* synthetic enzymatic biosystems might open the door to cost-effective biomanufacturing of laminaribiose from starch at an industrial scale.[21] However, these enzymes were all purified by Ni-NTA described in our previous study, but this purification process is not realistic for industrial applications. Because permeabilized whole cells after heat treatment at more than 60 °C are ideal catalysts for industrial enzymatic transformation,[64] enzymes for the subsequent transformation must withstand the heat treatment. In our previous *in vitro* biosystem for converting starch to laminaribiose, it was reported that the optimal temperatures for IA, αG, αGP, and PsLBP were 80, 70, 70 and 55 °C, respectively. Therefore, except for PsLBP, the enzymes could retain considerable activity during the preparation of permeabilized whole cells by heat treatment at >60 °C. Thus, we conducted a specific thermal stability test on the purified PsLBP. The T_m value of PsLBP determined using DSC was 64.4 °C (Figure 1b), and the $t_{1/2}$ of LBP at 60 °C was only about 10 min (Figure 1c). The experimental results showed that PsLBP was fragile and unstable at 60 °C. Therefore, enhancing the thermostability of PsLBP should benefit the industrial scale-up of the *in vitro* biosystem for laminaribiose production from starch.

Molecular Structure of PsLBP. PsLBP belongs to the GH94 family. Crystal structures of PsLBP have been successfully determined and assigned the PDB IDs of 6GH2, 6GH3, and 6GGY,[27] each of which contains different small molecules. Specifically, the small molecule in 6GH2 is G1P; in 6GH3, it is alpha-mannose-1-phosphate; and in 6GGY, it is a single sulfate molecule. Using 6GGY for illustration, PsLBP contains two identical subunits per asymmetric unit, sharing a similar $(\alpha/\alpha)_6$-barrel catalysis domain and several β-sandwiches. The colored region depicted in Figure S1 represents a monomeric unit of PsLBP comprising four domains, while the gray region signifies a different monomeric unit. Each PsLBP monomer consists of four domains, which are an N-terminal β-sandwich (residues 1−297; yellow); a helical linker region (residues 298−327; purple); an $(\alpha/\alpha)_6$ catalytic domain (residues 328−808; green), in which the catalytic pocket is present in red; and a C-terminal domain (residues 809−911; blue).

Computer-Aided Rational Design for Selecting Mutation Sites to Enhance the Thermostability of PsLBP. A hybrid approach was employed to address the issue of sampling bias by incorporating several complementary computational approaches of rational design, rather than relying solely on force field or phylogeny approaches. These methods introduced salt bridges and disulfide bonds, modified unfavorable surface charge-bearing amino acids, and filled structure cavities. The initial step in the hybrid strategy involved using coevolution analysis and a potential energy function to predict potentially stabilizing mutations across the entire protein sequence, followed by scoring all the mutations of amino acids based on the results of calculations from the complementary computational methods. Candidate sites with typical known pitfalls (such as disrupting pre-existing hydrogen bonds or salt bridges, or creating unreasonable hydrogen bonds or salt bridges) were eliminated, and the remaining predicted mutation sites were examined experimentally (Figure 2).

Previous studies showed that the presence of salt bridges formed between nearby residues with opposite charges could affect protein thermostability.[65,66] It was proposed that designing and constructing new salt bridges could effectively improve protein thermostability. We made attempts to introduce additional salt bridges using coevolution approach with the phylogeny-based technique, EVCoupling, which relies on evolutionarily conserved and encoded messages in multiple sequence alignments and implicitly simulates the interactions between all residue pairs in proteins that coevolved over time. Because coevolving pairs of amino acids are always close to each other spatially within the final three-dimensional structure of the protein,[67] we rationalized that the ECs harboring charged amino acid residues that naturally existed in PsLBP without forming salt-bridge bonds could be candidates to form additional salt bridges with an introduced residue with an opposite charge. Based on the above assumptions, we selected 14 promising residues to form new salt bridges, as shown in Figure S2. Among them, five amino acids (T117, T148, P275, L361, and A647) formed ECs with two positively charged residues. Accordingly, mutating of these five amino acids to negatively charged amino acids (D or E) may form new salt bridges to enhance protein thermostability.

As disulfide bonds have been found to be effective for enhancing protein stability, we used the PsLBP structure (PDB ID: 6GGY) and uploaded it to DbD2 to find potential pairs for the formation of disulfide bonds. The DbD2 identified a total of 111 potential pairs with a corresponding χ_3 torsion angle (−87° or 97 ± 30°), disulfide bond energy (more than 0 kcal/mol), and sum *B*-factors (more than 40). If any of these pairs showed evidence of coevolution indicated by shared ECs, they potentially facilitated the formation of disulfide bonds. Therefore, an initial comparison with ECs was conducted to identify regions of overlap, resulting in a reduction of the candidate pool to 34. Subsequently, the difference in Gibbs free energy change ($\Delta\Delta G$) between the WT and mutants, specifically related to the formation of disulfide bonds, was accurately determined using FoldX. This calculation was performed for the couples in which the selected amino acids were substituted with cysteines. Among the 34 pairs, only 12 pairs demonstrated negative $\Delta\Delta G$ values, indicating a high likelihood of forming disulfide bonds between these 12 pairs by introducing cysteine (Table S2).

Modification of unfavorable surface charge-bearing amino acids is a structure-based rational design approach that has been shown to be an effective method for thermostability improvement.[54,55,68−71] There are 263 charged residues on the surface of PsLBP. An ETSS was used to calculate the total interaction energy (E_{ij}) of each surface-charged amino acid of PsLBP. The 263 residues were renumbered and indexed (Table S3), with the corresponding total E_{ij} values represented by a bar chart in Figure S3a. A positive E_{ij} value indicated an unfavorable interaction, thus a total of 119 unique predicted sites shown in the green box of Figure S3a (residues with positively charged E_{ij}) were considered potentially stabilizing candidates, while 144 sites (residues with negatively charged E_{ij}) were identified as beneficial to the stability of the PsLBP protein and therefore were not mutated. Subsequently, three complementary tools, Gromacs for MD stimulation, B-FITTER for calculating *B*-factors, and ClustalW for sequence alignment, were utilized to comprehensively analyze PsLBP. The primary aim was to discern the relatively unstable and nonconserved amino acid residues among the 119 unfavorable

https://doi.org/10.1021/acssuschemeng.3c06089
ACS Sustainable Chem. Eng. XXXX, XXX, XXX−XXX

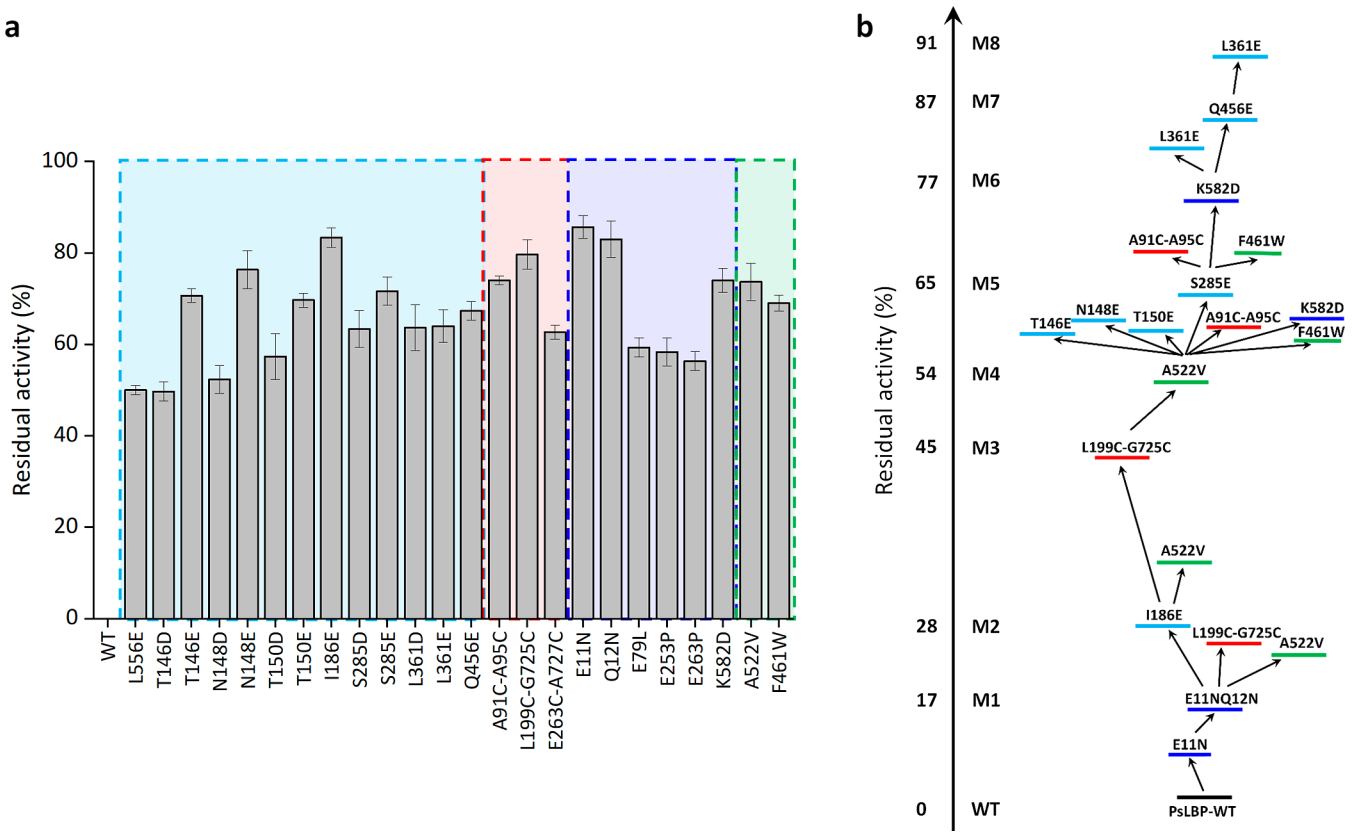

Figure 3. (a) Residual activity results of rationally designed mutants with improved thermostability. The candidates donated by different strategies were filled with different colors, *i.e.*, introducing salt bridges (light blue), introducing disulfide linkages (red), optimizing surface charge−charge interaction (blue), and filling structure cavities (green). The thermostability was presented as the residual activity after heat-treatment at 60 °C for 15 min. (b) Thermostability improvement progress of the mutants from M1 to M8 with combinatorial mutation sites. The thermostability was presented as the residual activity after heat-treatment at 60 °C for 30 min. All data are averages of three independent experiments with standard deviations.

surface charge-bearing residues. Then, the residues simultaneously exhibiting the most pronounced fluctuations within a particular local range on the basis of the *B*-factor and RMSF curves were highlighted with a green label, indicating that they were sites with a higher likelihood of enhancing stability (Figure S3b). Furthermore, three unique LBP sequences were aligned by the program ClustalW, and the conserved residues indicated that the mutations were unfavorable for enzyme activity (Figure S3c). Because there was a large number of candidates, we scored the amino acids based on a few key principles: residues with a positively charged E_{ij} scored 2 points, residues with a negatively charged E_{ij} scored −2 points, residues with a locally high RMSF value scored 2 points, residues with locally high *B*-factors scored 2 points, conserved residues in LBPs scored −2 points, and residues that established ECs with high-scoring residues while displaying close spatial proximity scored 6 points. After scoring, 35 mutation sites scoring 6 points were selected as candidate mutation sites. Finally, FoldX was employed to perform energy calculations and virtual saturation for all the mutation sites to identify the optimal amino acid at each site with the lowest $\Delta\Delta G$ value (Table S4).

Tight packing of side chains in protein cores is crucial to protein folding and stability. Defects in structure packing are associated with decreased stability, and therefore locating regions that are not well packed in the structure followed by identifying mutations to improve the packing should be very useful for improving the thermostability of the protein. PsLBP underwent iterative redesign using RosettaVIP. Based on domain analysis as depicted in Figure S1, the PsLBP protein consisting of 911 amino acids was categorized into five distinct groups to design cavities, in accordance with the online server's requirement of limiting the number of amino acids to less than 300. Detailed information regarding the grouping can be found in Table S5. Iterative procedures were applied to each component until no further mutation sites with lower $\Delta\Delta E$ values [a change of the VIP energy change (ΔE) value between the mutant and wild type; the smaller the $\Delta\Delta E$ value, the more stable the designed mutants] could be identified. Among the identified mutant variants, six variants from domains A, C, D, and E exhibited a $\Delta\Delta E$ energy below −5 kcal/mol, and notably, four variants exhibited a $\Delta\Delta E$ value lower than −10 kcal/mol. These mutations were predominantly selected during the initial one or two rounds of the calculation and were considered more likely to confer an enhanced folding efficiency to PsLBP. Group B was the only group that underwent five iterations, but overall, the $\Delta\Delta E$ values were relatively high, indicating that filling cavities in this group had a less pronounced effect. As a result, we successfully identified 11 mutation sites that exhibited negative $\Delta\Delta E$ energy and that may enhance protein packing (Table S5).

Filtering Chemically Unreasonable Mutations by Structural Inspection. Potentially stabilizing point mutations often have several off-target effects because of simplifications in

https://doi.org/10.1021/acssuschemeng.3c06089
ACS Sustainable Chem. Eng. XXXX, XXX, XXX−XXX

energy functions and incomplete conformational sampling. Eliminating such variants will improve the quality of the library that will subsequently be screened experimentally. Here, the virtual inspection process followed certain criteria to ensure the integrity of the mutations introduced. Specifically, it was imperative that the introduced residues should not disrupt essential hydrogen bonding or salt-bridge interactions and should be not within the hydrophobic catalytic pocket of the protein. For example, residue 58E (Table S4) was found to form a salt bridge with 177R in the WT structure. However, mutating residue 58E to P would have disrupted an existing salt-bridge interaction, potentially leading to increased instability of the enzyme. Therefore, this mutation site was excluded from further consideration. Based on the above-mentioned principles, 27 sites were excluded from the candidates, providing a final library of 59 candidates for mutations. All the mutations that were validated experimentally are summarized in Table S6.

PsLBP Mutants with Improved Thermostability. Based on the above analysis, using recombinant plasmid pET28a-PsLBP as the template, 59 mutants were constructed by site-directed mutagenesis using the primers listed in Table S6. After protein overexpression and harvesting by centrifugation, the cells harboring the recombinant mutants were lysed and heat-treated at 60 °C for 15 min, and the residual activity values were determined at 50 °C. Under the same conditions, PsLBP-WT lost its activity completely. After experimental validation, 19 well-expressed mutants developed from the four computational strategies of introducing salt bridges (highlighted in light blue), introducing disulfide linkages (highlighted in red), optimizing surface charge-bearing amino acids (highlighted in blue), and filling structural cavities (highlighted in green) showed increased stability (≥50% residual activity after being treated at 60 °C for 15 min) (Figure 3a).

Then, the mutation sites were combined to obtain PsLBP mutants with higher thermostability. Owing to epistatic effects, all positive mutations may not cooperate to achieve the desired function. Indeed, a PsLBP variant containing all 19 beneficial mutations was completely inactive. Then, the best individual of each strategy was chosen as the pacesetter (E11N, I186E, L199C-G725C, and A522V) to attract offspring for better combinatorial mutants (Figure 3b). After subjecting the aforementioned single-point mutants to thermal exposure at 60 °C for a duration of 15 min, a subset of them demonstrated the capacity to preserve over 80% of their functional activity. Consequently, the analysis of thermal stability in the subsequent combinatorial mutation process necessitated extending the heat treatment duration to 30 min. Because E11N was the most thermostable mutant and Q12N was among the top five mutants and adjacent to E11N, they were combined as M1, the thermostability of which was higher than that of either E11N or Q12N. Then, an iterative mutagenesis methodology was employed, and the most thermostable mutant was selected for the next round of mutagenesis. In the first round, three other mutation sites (I186E, L199C-G725C, and A522V) were individually incorporated into M1. The most thermostable mutant, M1-I186E, was designated as M2. Progressing from M2, the remaining two mutation sites (L199C-G725C and A522V) were introduced into M2 during the second round, wherein M2-L199C-G725C demonstrated superior thermostability compared to M2-A522V. Consequently, M2-L199C-G725C was designated as M3. Then, A522V was incorporated into M3 to yield M4. The stepwise addition of these mutation sites correlated with an improvement in the thermostability of the mutants from M1 to M4. Subsequently, the pacesetters began attracting offspring mutations from each strategy. Within the light blue group, four candidates (T146E, N148E, T150E, and S285E) exhibited nearly equal performance in improving thermostability. In the blue group, K582D was a suboptimal mutant, and A91C-A95C and F461W were selected from the red and green groups, respectively. After carefully comparing these seven candidates on M4, it was found that S285E exhibited the best performance, yielding M5. Although T146E, N148E, and T150E were structurally compatible with each other, attempts to combine them individually with M5 or to combine them were unsuccessful in improving stability beyond that of M5. Afterward, we attempted to individually combine A91C-A95C, K582D, and F461W with M5. It was found that K582D had the best thermostability among these three mutations, yielding M6, and we found that A91C-A95C and F461W, whether combined individually or in pairs with M6, failed to further improve the thermostability. In a final round of incorporating other mutations into M6, only Q456E and L361E from the light blue group were found to further enhance thermostability, resulting in M7 and M8. Finally, M8 retained 91% residual activity after heat treatment at 60 °C for 30 min. Attempts to integrate mutants from the other three groups had a negative impact, causing a loss of enzyme activity, a decrease in thermal stability, or adverse expression of the enzyme.

Property Characterization of the Wild-Type and Mutant Enzymes. To gain a deeper insight into the mutagenesis effects of these 10 mutation sites on the characteristics of the enzyme, the thermostabilities, specific activity values, and optimal temperatures of the mutants were examined. To assess the thermostability of the WT and variant enzymes, their $t_{1/2}$ and T_m values were determined. For the $t_{1/2}$ measurement, the enzymes were preincubated at 60 °C in 50 mM HEPES buffer (pH 7.0). As shown in Figure 4a and Table 1, the $t_{1/2}$ value of PsLBP-WT was ∼10 min at 60 °C. In contrast, all the mutants showed higher $t_{1/2}$ values than the wild type and the M8 mutant demonstrated the best $t_{1/2}$ value, which was 12.1 h, representing a 71.11-fold improvement over the WT enzyme. Subsequently, the T_m values of the WT and variant enzymes were determined using DSC (Table 1 and Figure 4b). As shown in Table 1, the T_m of PsLBP-WT was measured to be 64.4 °C. The T_m difference was about 3 °C in each round from M1 (lowest) to M4 (highest) and about 1 °C in each round from M4 (lowest) to M8 (highest); thus, the M8 mutant showed the highest T_m of 79.7 °C (Figure 4b), about 15 °C higher than that of the WT, indicating that the strategy we designed enabled us to engineer PsLBP with enhanced thermostability. Then, the optimal reaction temperatures of the WT enzyme and M8 mutant in the temperature range of 40−80 °C in 50 mM HEPES buffer (pH 7.0) were investigated. The optimal temperature for the PsLBP-M8 enzyme was found to be 70 °C, about 15 °C higher than that of PsLBP-WT. Although the specific activity of the M8 mutant at its optimal temperature was about 20% lower than that of the WT, the specific activity of the M8 mutant at 60 °C was about 2.4-fold higher than that of the WT because of the enhanced thermostability of the M8 mutant (Figure 4c).

The kinetic parameters of the WT enzyme and the mutant enzymes at 60 °C were determined using the Michaelis−Menten kinetic equation (Table 1). The K_m values of the variant enzymes had no obvious difference with those of the

https://doi.org/10.1021/acssuschemeng.3c06089
ACS Sustainable Chem. Eng. XXXX, XXX, XXX−XXX

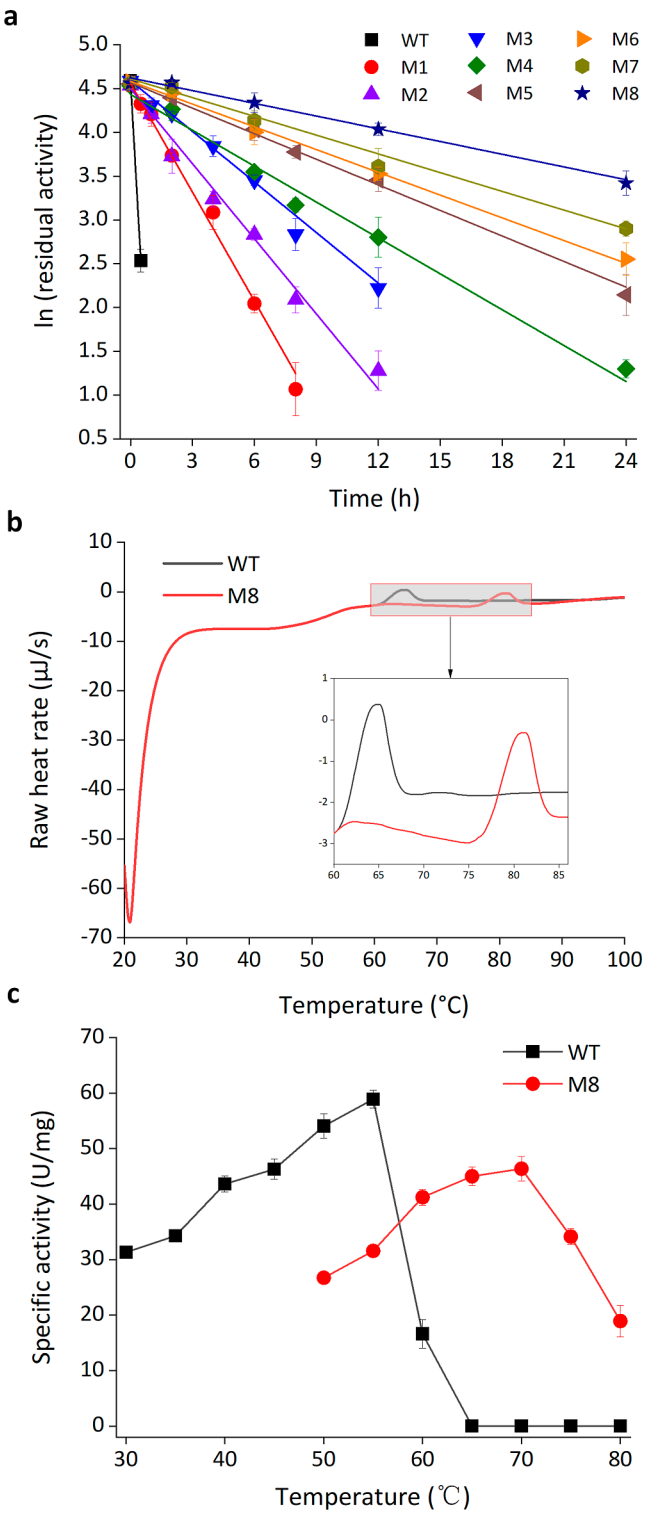

Figure 4. (a) Half-life determination of purified PsLBP-WT and its variants at 60 °C. (b) DSC scan curves of purified PsLBP-WT and M8. (c) Temperature-dependence profiles of specific activities of PsLBP-WT (square) and M8 (circle). All data are averages of three independent experiments with standard deviations.

WT enzyme, while the catalytic efficiency (k_{cat}/K_m) values were increased from 2.3- to 3.0-fold of that of the WT enzyme. In comparison to the other mutants, M4 had the highest catalytic efficiency, and the k_{cat}/K_m values of the mutants following M4 (M5−M8) decreased to different degrees,

Table 1. Characteristics of PsLBP-WT and Its Variants[b]

enzymes	mutations	$t_{1/2}$ (h)	fold	T_m	$K_{m,Glc}$ (mM)	$k_{cat,Glc}$ (s^{-1})	$k_{cat,Glc}/K_{m,Glc}$ (s^{-1}/mM)	$K_{m,G1P}$ (mM)	$k_{cat,G1P}$ (s^{-1})	$k_{cat,G1P}/K_{m,G1P}$ (s^{-1}/mM)
PsLBP-WT	WT	0.2	1.0	64.4	1.3[a]	72.3[a]	54.4[a]	1.0[a]	72.3[a]	71.6[a]
PsLBP-M1	E11N/Q12N	1.6	9.2	66.2	1.4	50.9	36.1	1.1	51.1	46.1
PsLBP-M2	E11N/Q12N/I186E	2.6	15.2	69.1	1.4	59.4	43.7	1.2	59.4	51.2
PsLBP-M3	E11I/Q12V/I186E/L199C/G725C	3.5	20.4	72.7	1.5	61.9	41.6	1.1	62.1	56.9
PsLBP-M4	E11I/Q12V/I186E/L199C/G725C/A322V	5.1	30.2	75.1	1.2	64.5	52.8	1.0	64.3	66.3
PsLBP-M5	E11I/Q12V/I186E/L199C/G725C/A322V/S285E	7.7	45.5	76.3	1.3	59.6	46.2	0.9	58.9	63.3
PsLBP-M6	E11I/Q12V/I186E/L199C/G725C/A322V/S285E/K582D	9.1	53.6	77.1	1.1	58.5	51.3	1.0	58.1	56.4
PsLBP-M7	E11I/Q12V/I186E/L199C/G725C/A322V/S285E/K582D/Q456E	10.4	61.3	78.0	1.3	56.7	42.9	1.0	56.8	55.6
PsLBP-M8	E11I/Q12V/I186E/L199C/G725C/A322V/S285E/K582D/Q456E/L361E	12.1	71.1	79.7	1.2	53.2	42.9	1.1	53.1	49.6

[a]Steady-state kinetics of PsLBP-WT were measured in 100 mM HEPES buffer (pH 7.5) containing 5 mM $MgCl_2$ with a variety of concentrations of Glc and G1P (0.5−5 mM) at 50 °C. [b]Steady-state kinetics of PsLBP-WT and mutants were measured in 100 mM HEPES buffer (pH 7.5) containing 5 mM $MgCl_2$ with a variety of concentrations of Glc and G1P (0.5−5 mM) at 60 °C.

https://doi.org/10.1021/acssuschemeng.3c06089
ACS Sustainable Chem. Eng. XXXX, XXX, XXX−XXX

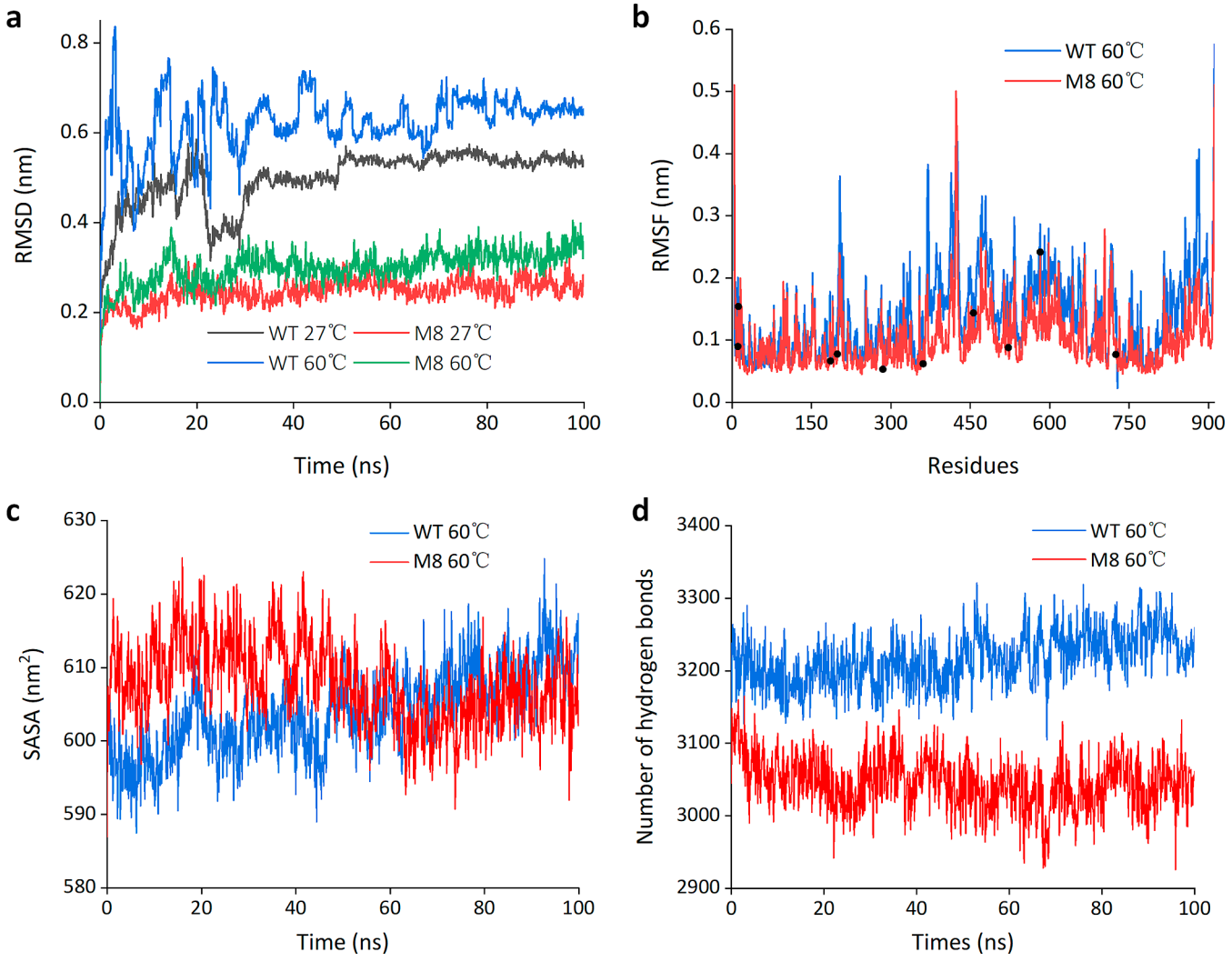

Figure 5. Changes of PsLBP-WT and M8 structures during the MD simulation. (a) Average C_α rmsd at 27 and 60 °C. (b) Average backbone RMSF at 60 °C. (c) SASA at 60 °C. (d) Number of hydrogen bonds at 60 °C.

indicating the trade-off between thermostability and specific activity.[72,73] The multiple strategies resulted in a highly stable mutant that could be employed to test and verify its performance for laminaribiose production under industrial conditions.

MD and Conformational Stability Analysis of PsLBP-M8. To explore the structural mechanism of the M8 mutant with enhanced thermal stability, MD simulations of PsLBP-WT and PsLBP-M8 were performed at 300 and 333 K for 100 ns. The structure of PsLBP-WT for MD was the crystal structure of 6GGY (PDB ID) without the substrate, and AlphaFold 2, a software tool renowned for its predictive capabilities, predicted the structure of the M8 mutant without the substrate. The obtained structures were used to calculate the rmsd, RMSF, SASA, and the total number of hydrogen bonds. The rmsd is reported as an important parameter for estimating the thermal fluctuation of the protein conformation. Protein thermostability is negatively correlated with the rmsd value and positively related to the protein rigidity. In the present study, time profiles of the rmsd based on the entire 100 ns simulated trajectory were recorded. As depicted in Figure 5a, the rmsd values of both PsLBP-WT at 27 and 60 °C were higher than those of PsLBP-M8 over a 100 ns simulation, respectively, and the rmsd values of PsLBP-WT at 27 °C were even higher than those of PsLBP-M8 at 60 °C. Considering the equivalent simulation time, PsLBP-M8 exhibited both a faster convergence speed and lower fluctuation compared to the WT enzyme, indicating that PsLBP-M8 had a much higher thermostability than the PsLBP-WT enzyme. Moreover, to explore the structural flexibility of the full protein, we determined the RMSF of all C_α atoms of the protein. RMSF analysis revealed information on the regions with enhanced flexibility of the protein. The average fluctuations in the coordinates of individual residues obtained by different force fields were measured. Figure 5b shows that the overall RMSF values of the PsLBP-M8 system were lower than those of the PsLBP-WT system at 60 °C. Notably, the black-marked points in this figure represent all the mutated positions in the PsLBP-M8 system, and it can be observed that the RMSF values of these positions were consistently lower than those of PsLBP-WT, indicating the reduced fluctuations and increased stability in these regions of the M8 mutant. However, this phenomenon was not as evident under normal temperature conditions, as the essential flexible regions in both the PsLBP-WT and PsLBP-M8 systems exhibited minimal changes during the simulations conducted at 27 °C (Figure S4).

https://doi.org/10.1021/acssuschemeng.3c06089
ACS Sustainable Chem. Eng. XXXX, XXX, XXX−XXX

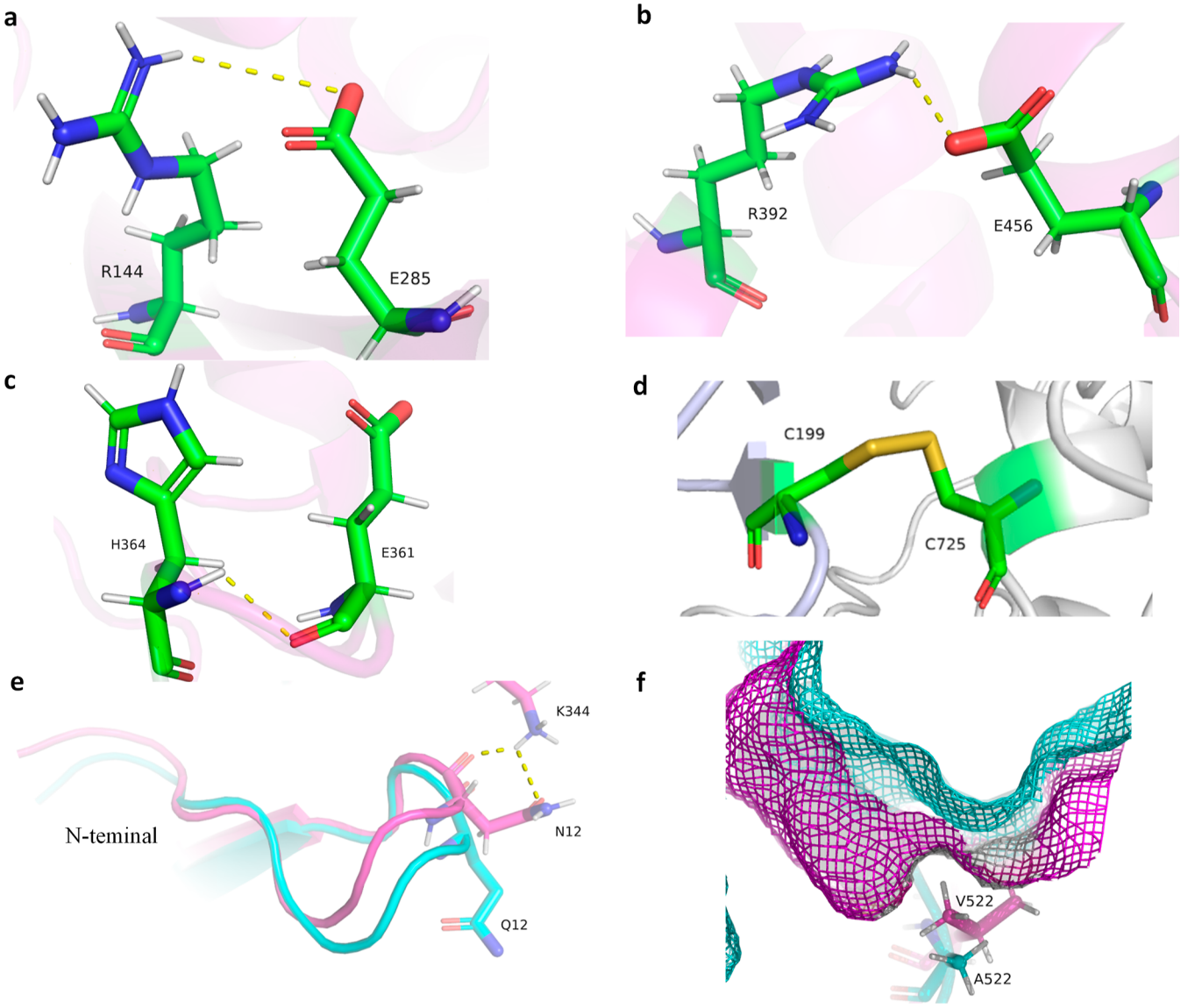

Figure 6. Structural analysis of the PsLBP-WT and M8. (a) Interaction analysis diagram of E285 and R144 of M8. (b) Interaction analysis diagram of E456 and R392 of M8. (c) Interaction analysis diagram of E361 and H364 of M8; the yellow dashes in A, B, and C indicate a salt bridge. (d) Interaction analysis diagram of the C199 in monomer A and C725 in monomer B of M8; the yellow sticks indicate a disulfate bond. (e) Difference between the superimposed structures of PsLBP-WT (cyan) and M8 (purple) at positions 11 and 12. (f) Comparison of the surface distortions at position 522 between PsLBP-WT (cyan) and M8 (purple). The protein surfaces are identified by "mesh" and "surface" in corresponding colors.

The SASA of a protein is also considered a critical factor in assessing its stability. SASA is defined as the surface area around the protein that is accessible to a solvent sphere with the van der Waals contact surface. We assessed the time-dependent SASA of all protein residues to ascertain the protein's adjustability and to clarify its solvent availability. It was observed that the SASA of the WT system started around 600 nm^2 and rose slightly to 610 nm^2 over the course of 50−75 ns before leveling off (Figure 5c). The increase in SASA implied that the equilibrium conformation of the WT enzyme shifted to a partially unfolded state. In contrast, the M8 system fluctuated from 610 nm^2 initially, dropped to 600 nm^2 at 50 ns, and then remained at that level. It can be inferred that less surface area of the M8 mutant was exposed to the solvent medium and more residues of the M8 mutant became buried inside the protein core.[74]

A solvated protein experiences intrapeptide and water−peptide hydrogen bonds. The number of these hydrogen bonds may also correlate with protein thermostability. As PsLBP is a large homodimer protein with a tremendous surface area, water−peptide hydrogen bonds[74] are the main contribution to the total hydrogen bonds. Estimation of the number of such hydrogen bonds gives an understanding of the conformational stability and rigidity of the protein structure. It also helps in understanding the dynamics of the protein. The time evolution of hydrogen bonds over the simulation period is shown in Figure 5d. The number of water−peptide hydrogen bonds of PsLBP-WT was higher than that of PsLBP-M8, indicating the higher conformational stability and rigidity of the M8 structure.

Detailed Microenvironmental Structural Analysis for Improved Thermostability of PsLBP. To gain insights into the impact of mutations on stabilizing PsLBP, the equilibrium

https://doi.org/10.1021/acssuschemeng.3c06089
ACS Sustainable Chem. Eng. XXXX, XXX, XXX−XXX

structures of PsLBP-WT and PsLBP-M8 were obtained after 100 ns of MD simulation at 60 °C. Superposition of the PsLBP-WT and PsLBP-M8 dimers revealed a very close structural similarity with an rmsd value of 0.205 Å for 1822 C_a atoms. To confirm the effectiveness of our design strategy, we initially examined the formation of salt bridges in the structures. Based on the EVCoupling prediction, PsLBP-M8 formed four additional salt bridges with the mutations, while only three ones succeeded between E285 and R144 (Figure 6a), E456 and R392 (Figure 6b), E361 and H364 (Figure 6c), thereby increasing the thermostability of the enzyme. However, the mutation sites E186 and H184 failed to form a pair, but they also improved the thermostability, as the β-sheet containing E186 lifted to approach the residue Y265, which is located inside the protein, resulting in a better package and a more stable status (Figure S5a).

Next, we proceeded to assess the efficacy of the second strategy through an investigation into the presence of newly formed disulfide bonds in PsLBP-M8. As indicated in Table S2, residue 199 of one monomer and residue 725 of the other monomer were predicted to form a disulfide bond at the interface of the PsLBP dimer; then, upon mutating both residue 199 and residue 725 to cysteines, two pairs of disulfide bonds could potentially be established per dimer. To ascertain the formation of these new disulfide bonds in the L199C-G725C mutants of PsLBP-M8, we employed the DTNB titration method to analyze the protein's free thiols before and after treatment with DTT. DTNB, a reagent that reacts specifically with free thiol groups in proteins, generates 5-thio-2-nitrobenzoic acid, which can be quantified by measuring absorbance at 412 nm. After treatment with DTT, cysteine residues participating in disulfide bonds are reduced, resulting in the formation of two additional free thiols. As shown in Table S7, the number of free thiols of PsLBP-M3 and M8 was the same as that of PsLBP-WT, even though PsLBP-M3 and M8 contained two more cysteines than PsLBP-WT. After DTT treatment of these three enzymes, the free thiol number of PsLBP-WT did not increase, whereas the free thiol number of M3 and M8 increased by ∼4 for the dimer enzyme. These results indicated the formation of two disulfide bonds between L199C and G725C of the PsLBP-M3 and M8 mutants. Moreover, the existence of the disulfide bond was corroborated by AlphaFold 2. The software also predicted the formation of two disulfide bonds at the interface between the two monomers, with 199C in monomer A interacting with 725C in monomer B, and 725C in monomer A interacting with 199C in monomer B (Figures 6d and S5b). Based on the aforementioned results, we concluded that the formation of new disulfide bonds at the interface between monomers should contribute to the enhanced thermostability observed in the mutants with L199C-G725C. Moreover, considering the values in Table S2, the $\Delta\Delta G$ of the 199C-725C mutant is the lowest. This result suggested that when deciding to introduce disulfide bonds for enhanced stability, it may be preferable to favor combinations with the lowest postmutation $\Delta\Delta G$.

The enhancement of thermal stability through engineering adverse surface-charged residues can be attributed to the formation of additional hydrogen bonds within the protein structure. For example, in PsLBP-M8, D582 may form an additional C^{δ}-COO hydrogen bond with P583 (Figure S6a),[75] whereas no discernible interactions were observed between K582 and neighboring residues in PsLBP-WT (this analysis was conducted using PyMOL). Moreover, the K582D mutation induced alterations in the local charge environment and facilitated the formation of more hydrogen bonds, which likely contributed to the increased thermostability. For the E12N mutation, beyond demonstrating a hydrogen bond with E14, a feature shared with PsLBP-WT, it also engaged in additional hydrogen bonds with K344 (Figure S6b). This hydrogen bonding arrangement potentially results in an augmented N-terminal compaction of loop 1 (amino acids 1−15) in comparison to PsLBP-WT (Figure 6e). These structural changes promoted the acquisition of a more compact protein conformation, consequently augmenting the protein's resistance to the elevated temperatures.

Finally, alterations in spatial configurations also contributed to the enhancement of stability. The incorporation of a strategically designed single-point mutation, A522V, predicted by Rosetta VIP, represented a promising approach for augmenting the stability of the mutant. As depicted in Figure 6f, the substitution of Ala with Val at position 522 induced significant conformational changes, resulting in a notable surface distortion of PsLBP-M8. Notably, the presence of the bulkier side chain of Val contributed to a more compact structural arrangement in the mutant variant. As evidenced in Figure S6c, the hydrogen bonding between G521 and R428 established a prominent interaction on the protein surface, whereas A522 in the PsLBP-WT protein resided internally, distanced from the cyan surface. However, as revealed in Figure S6d, the larger side chain of V522 induced structural alterations in the nearby region, concomitantly forming the magenta surface of PsLBP-M8 in conjunction with G521 and R428. These alterations significantly contributed to a more compact conformation of the protein. This structural modification holds significant potential for improving the overall stability and functional properties of the mutant.

In summary, our combinational rational strategy was effective in enhancing the stability of a large enzyme, PsLBP, and most of the contributions of the designed mutations to the thermostability were consistent with our expectations.

Laminaribiose Production by *In Vitro* Synthetic Enzymatic Biosystems under Industrial Conditions Using Permeabilized Whole Cells as Catalysts. Because all the enzymes for the conversion of starch to laminaribiose could tolerate the heat treatment at 60 °C, including PsLBP-M8, heat-treated whole cells were used for biotransformation in this study. Four *E. coli* whole cells of pET28a-TmαGP, pET28a-BsαG, pET28a-PsLBP-WT, and pET28a-PsLBP-M8 plasmids were collected after centrifugation of the culture medium. Then, the whole cells with an OD_{600} of 100 were treated at different temperatures ranging from 50 to 70 °C for 20 min, followed by the addition of 100 g·L^{-1} of IA-treated maltodextrin for laminaribiose production at 60 °C. According to the model simulations in our previous research,[21] the optimal loading amounts for laminaribiose production by the *in vitro* enzymatic biosystem were 5.1 U/mL αGP, 2.5 U/mL αG, and 6.7 U/mL PsLBP. Based on these enzyme units for the reaction, the loading amounts of the whole cells were determined from the expression level of each enzyme. The expression levels of these enzymes ranged from 35 to 40%, and the lowest values were employed to calculate the loading amounts of the whole cells. In the whole-cell cocktail containing the PsLBP-WT system, we introduced 5.3 OD/mL of heat-treated TmαGP cells and 0.7 OD/mL of heat-treated BsαG cells, accompanied by 7.7 OD/mL of heat-treated PsLBP-WT cells. In the whole-cell cocktail containing

https://doi.org/10.1021/acssuschemeng.3c06089
ACS Sustainable Chem. Eng. XXXX, XXX, XXX−XXX

the PsLBP-M8 system, equal loading amounts of heat-treated TmαGP and BsαG cells were added, along with 3.2 OD/mL of heat-treated PsLBP-M8 cells. The cells without heat treatment were used as controls. As shown in Figure 7a, for the whole-cell cocktail containing PsLBP-WT, the highest laminaribiose titer occurred when the cells were heat-treated at 55 °C before the reaction, and higher treatment temperatures decreased the product titer because of the poor stability of PsLBP-WT at 60 °C. For the whole-cell cocktail containing PsLBP-M8, the laminaribiose titers produced by all the heat-treated cells at the tested temperatures were all much higher than those of the untreated cells and PsLBP-WT cells. This result further confirmed that PsLBP-M8 had a much higher thermostability than the WT enzyme. The PsLBP-M8 cells treated at 70 °C had the highest laminaribiose titer among all the test temperatures, about 3.3 times that of untreated cells (Figure 7a). As a result, the whole-cell heat treatment condition for laminaribiose production was set at 70 °C for 20 min before the reaction at 60 °C.

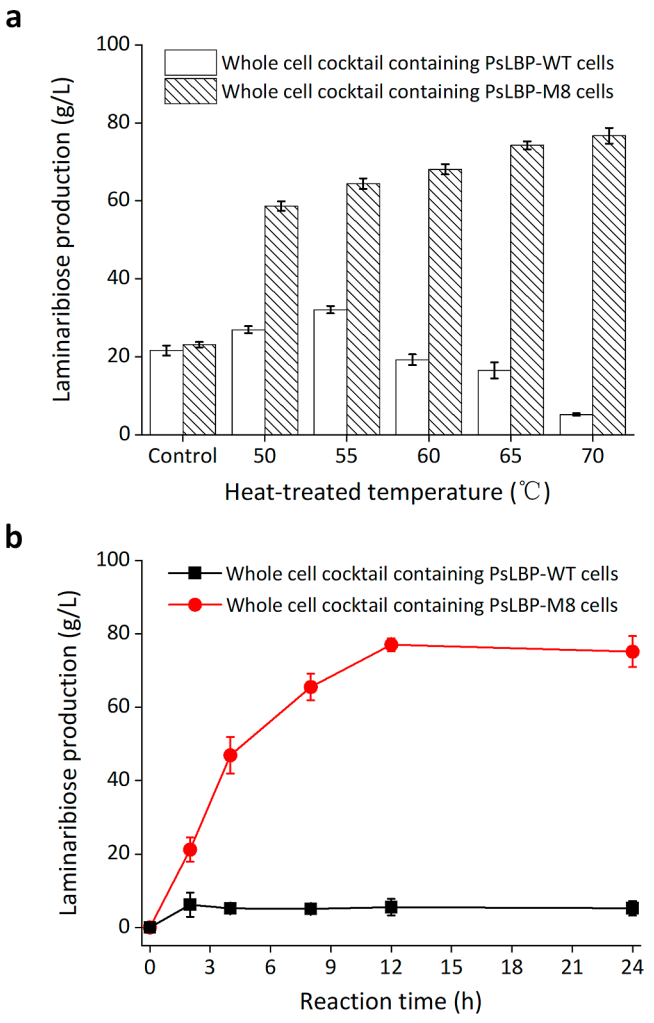

Figure 7. Laminaribiose production from 100 g/L of the debranched maltodextrins by *in vitro* synthetic enzymatic biosystems containing αGP, αG, and PsLBP-WT or M8 through permeabilized whole-cell bioconversion. (a) Effect of permeabilization of *E. coli* whole cells at different temperatures on the production of laminaribiose. The whole cells without any treatment were used as a control. (b) Time-dependence profiles of laminaribiose production by the *in vitro* biosystems containing αGP, αG, and PsLBP-WT (square) or M8 (circle) using permeabilized whole cells, which were treated at 70 °C for 20 min. All data are averages of three independent experiments with standard deviations.

The performance of the *in vitro* biosystem containing PsLBP-WT and PsLBP-M8 for laminaribiose production from IA-treated maltodextrin was evaluated at 60 °C after the whole cells were subjected to a 70 °C heat treatment for 20 min (Figure 7b). The *in vitro* biosystems (50 mL) with PsLBP-WT and M8 mutant cells generated 14.8 mM (5.1 g/L, molar yield of 4.3%) and 225.5 mM (77.2 g/L, molar yield of 75.0%) of laminaribiose from 100 g/L IA-treated maltodextrin, respectively. Additionally, when we scaled up the reaction system containing PsLBP-M8 in a proportional manner to 30 L, the produced laminaribiose concentrations remained at ∼77.0 g/L, indicating the easy scale-up of the *in vitro* biosystem. Therefore, mutant M8 is considered to be adaptable for the industrial-scale production of laminaribiose from starch in our designed *in vitro* biosystem. Based on our observations, the occurrence of the Maillard reaction in our laminaribiose production was minimal. This can be attributed to the appropriate enzyme ratio, which prevented the generation of high concentrations of glucose that could easily lead to the Maillard reaction.

DISCUSSION

To promote the industrial application of laminaribiose, research to improve the reactivity or thermostability of crucial and underperforming enzymes *via* protein engineering has become a top priority. PsLBP was the most heat-sensitive enzyme in the *in vitro* biosystem for laminaribiose production. However, engineering PsLBP was challenging because it is a large dimeric enzyme with 911 amino acids in only one monomer by random mutagenesis on the whole sequence. In this study, we fulfilled the task of improving the thermostability of this large enzyme by combining four complementary rational approaches: introducing salt bridges, introducing disulfide linkages, optimizing surface charge-bearing amino acids, and filling structure cavities (Figure 2). Through this computational-guided rational design, compared to the WT enzyme, the $t_{1/2}$ and T_m values of the optimal PsLBP-M8 increased by 71.11-fold, and 15.3 °C, respectively, and the catalytic efficiency of M8 at 60 °C was also much higher than that of the WT enzyme. These findings suggest that a combination of computational methods for rational design can serve as a robust framework for engineering the thermostability of large proteins, such as LBP. After integrating the M8 mutant, rather than PsLBP-WT, into the *in vitro* laminaribiose production system at 60 °C, the heat-treated whole-cell cocktail containing PsLBP-M8 could convert 100 g/L starch into ∼77.0 g/L laminaribiose with a molar yield of ∼75.0%, providing a cost-efficient method for industrial-scale production of laminaribiose, a compound with various applications in the food and pharmaceutical industries. This study has the potential to substantially reduce the production cost of laminaribiose to $2000−3000 per ton and enhance its market value significantly.

In addition to the cumulative beneficial effects on the thermostability of the introduced mutation sites, changes in the secondary structure resulting from these mutation sites may have also contributed to the thermostability of LBP. Therefore, we computed the fractions of secondary structures of the protein using the do_dssp tool. The population of secondary structures is defined as the distribution of the total number of

https://doi.org/10.1021/acssuschemeng.3c06089
ACS Sustainable Chem. Eng. XXXX, XXX, XXX−XXX

residues forming the structure during the simulation present in the crystal structure. Moreover, from the virtual inspection of Figure S7a−c, it can be seen that there were few changes in the total secondary structure of PsLBP-WT and M8, with only a small decrease in the number of new α-helices and a slight increase in the amount of turns (labeled with black circles in Figure S7c) of the PsLBP-M8 mutant. This was consistent with what Mohd *et al.*[76] reported, in which the substitutions of one or a few amino acids that lead to the improvements in thermostability and optimal temperature of the mutants did not cause a substantial change in the secondary structures of the enzymes. This meant that the difference in thermostability between the WT enzyme and mutant M8 could not be attributed to the change in the secondary structure. Furthermore, there is often a trade-off between enzyme activity and stability during protein engineering. This is especially true for PsLBP, in which increasing stability may result in decreased activity and vice versa. However, because of the higher thermostability, the engineered thermostable enzyme exhibited higher activity at high temperatures. PsLBP-M8 exhibited about a 2.4-fold higher activity than the WT at 60 °C, making M8 a favorable option for industrial laminaribiose production.

Although PsLBP-M8 with increased thermostability was designed for the industrial production of laminaribiose and the mechanisms of the mutation sites of PsLBP-M8 were analyzed, several limitations remain to be addressed. (1) The limited number of successful outcomes reflects the relatively low success rate of our rational design. The main challenges in rational protein design stem from the reliance on theoretical models and variables such as protein−protein interactions, solvent effects, and allosteric regulation.[40] The development of artificial intelligence (AI) could provide a solution to overcome this challenge.[77] (2) To further enhance the thermostability of PsLBP or other oligosaccharide phosphorylases for the biomanufacturing of value-added oligosaccharides, the following steps can be considered, implementing an *in situ* high-throughput screening method to quickly identify stable mutants and utilizing or developing AI-aided strategies such as deep learning to improve the accuracy of rational design based on high-throughput data.[44,78] (3) The multiple enzymes for laminaribiose production can be coimmobilized using carrier-bearing or carrier-free modes. The use of polypeptide interactions for carrier-free immobilization, including SpyCatcher/SpyTag and dockerin/cohesin, is a highly effective approach to stabilizing multienzyme complexes.[79] This method directly links the enzyme components together, protecting the complex from denaturation and degradation, and exhibits significant potential for applications in industrial biotechnology and bioremediation.

In summary, a thermostable mutant (M8) of PsLBP was obtained *via* protein engineering based on a combined computer-aided rational design strategy. Compared with PsLBP-WT, the PsLBP-M8 exhibited much higher thermostability in terms of half-lives and T_m, along with much higher activity at 60 °C. Additionally, we demonstrated the application of PsLBP-M8 in an *in vitro* laminaribiose-producing biosystem at 60 °C with excellent biocatalytic performance under industrial conditions using heat-treated whole cells as catalysts. The accessibility of this engineering approach should provide unique strategies and research guidelines for the effective rational design of rate-limiting enzymes in enzyme cascades, further expanding the scope of *in vitro* biomanufacturing.

■ ASSOCIATED CONTENT

Supporting Information

The Supporting Information is available free of charge at https://pubs.acs.org/doi/10.1021/acssuschemeng.3c06089.

Additional material pertaining to experimental results; crystal structure of PsLBP-WT; coevolutionary analysis of PsLBP-WT; ETSS, RMSF, B-FITTER, and MSA analysis of PsLBP-WT; RMSF analysis of PsLBP-WT and M8; structural distinction at position 186 and the disulfide bond location; comprehensive analysis of the interactions of PsLBP-WT and M8; DSSP analysis of PsLBP-WT and M8; primers used for cloning and site-directed mutagenesis of PsLBP-M8; mutation sites predicted by DbD2; description of the indexing and corresponding residues in the ETSS calculation results; mutation sites predicted by ETSS; mutation sites predicted by Rosetta VIP; mutation candidates chosen for experimental validation; and determination of the number of free thiols and disulfide bonds (PDF)

■ AUTHOR INFORMATION

Corresponding Author

Chun You − *Tianjin Institute of Industrial Biotechnology, Chinese Academy of Sciences, Tianjin 300308, People's Republic of China; University of Chinese Academy of Sciences, Beijing 100049, People's Republic of China; National Center of Technology Innovation for Synthetic Biology, Tianjin 300308, People's Republic of China; In Vitro Synthetic Biology Center, Tianjin Institute of Industrial Biotechnology, Chinese Academy of Sciences, Tianjin 300308, People's Republic of China;* orcid.org/0000-0003-2305-336X; Email: you_c@tib.cas.cn

Authors

Shangshang Sun − *Tianjin Institute of Industrial Biotechnology, Chinese Academy of Sciences, Tianjin 300308, People's Republic of China; National Center of Technology Innovation for Synthetic Biology, Tianjin 300308, People's Republic of China; In Vitro Synthetic Biology Center, Tianjin Institute of Industrial Biotechnology, Chinese Academy of Sciences, Tianjin 300308, People's Republic of China;* orcid.org/0000-0001-9828-2488

Qiangzi Li − *Tianjin Institute of Industrial Biotechnology, Chinese Academy of Sciences, Tianjin 300308, People's Republic of China*

Lin Fan − *Tianjin Institute of Industrial Biotechnology, Chinese Academy of Sciences, Tianjin 300308, People's Republic of China; National Center of Technology Innovation for Synthetic Biology, Tianjin 300308, People's Republic of China; In Vitro Synthetic Biology Center, Tianjin Institute of Industrial Biotechnology, Chinese Academy of Sciences, Tianjin 300308, People's Republic of China*

Yi-Heng P. Job Zhang − *Tianjin Institute of Industrial Biotechnology, Chinese Academy of Sciences, Tianjin 300308, People's Republic of China; National Center of Technology Innovation for Synthetic Biology, Tianjin 300308, People's Republic of China; In Vitro Synthetic Biology Center, Tianjin Institute of Industrial Biotechnology, Chinese Academy of Sciences, Tianjin 300308, People's Republic of China*

https://doi.org/10.1021/acssuschemeng.3c06089
ACS Sustainable Chem. Eng. XXXX, XXX, XXX−XXX

Complete contact information is available at:
https://pubs.acs.org/10.1021/acssuschemeng.3c06089

Author Contributions

C.Y. proposed the idea of improving the thermostability of PsLBP. S.S. designed and performed enzyme engineering, enzymatic characteristic, and laminaribiose production experiments. L.F. performed enzymatic characteristics and DSC. S.S. and Q.L. conducted the MD simulation. S.S., C.Y., and Y.-H.P.J.Z. analyzed the data and drafted the manuscript. All authors discussed the results and commented on the manuscript.

Notes

The authors declare no competing financial interest.

■ ACKNOWLEDGMENTS

This work was supported by the National Key Research and Development Program of China (2021YFA0910601), National Natural Science Foundation of China (grant no. 32101009, 32022044 and 32271473), China Postdoctoral Science Foundation (2021M693354), and Tianjin Synthetic Biotechnology Innovation Capacity Improvement Project (grant no. TSBICIP-CXRC-051). The authors wish to acknowledge Jie Zhang for her help in guiding DSC operation and data processing.

■ REFERENCES

(1) Sun, S.; Wei, X.; You, C. The construction of an in vitro synthetic enzymatic biosystem that facilitates laminaribiose biosynthesis from maltodextrin and glucose. *Biotechnol. J.* **2019**, *14* (4), No. e1800493.

(2) Rahman, S.; Davids, M.; van Hamersveld, P. H. P.; Welting, O.; Rahaoui, H.; Schuren, F.; Meijer, S. L.; van den Wijngaard, R. M.; Hakvoort, T. B. M.; de Jonge, W. J.; Heinsbroek, S. E. M. Dietary Curdlan enhances bifidobacteria and reduces intestinal inflammation in mice. *Nutrients* **2021**, *13* (4), 1305−1322.

(3) Nishitani, Y.; Zhang, L.; Yoshida, M.; Azuma, T.; Kanazawa, K.; Hashimoto, T.; Mizuno, M. Intestinal anti-inflammatory activity of lentinan: influence on IL-8 and TNFR1 expression in intestinal epithelial cells. *PLoS One* **2013**, *8* (4), No. e62441.

(4) Shukla, S.; Park, J.; Park, J. H.; Lee, J. S.; Kim, M. Development of novel Meju starter culture using plant extracts with reduced Bacillus cereus counts and enhanced functional properties. *Sci. Rep.* **2017**, *7* (1), 11409−11421.

(5) Yvin, J.-C.; Levasseur, F.; Thanh, K.-N. T.; Le Bui, V. Composition and process for the stimulation and germination of grains of pollen. U.S. Patent 6,303,587 B1, 1999.

(6) Wang, L.-X.; Sakairi, N.; Kuzuhara, H. Peracetylated laminaribiose: preparation by specific degradation of curdlan and its chemical conversion into N-acetylhyalobiuronic acid. *Carbohyd. Res.* **1991**, *219*, 133−148.

(7) Sanz, M. L.; Gibson, G. R.; Rastall, R. A. Influence of disaccharide structure on prebiotic selectivity in vitro. *J. Agric. Food Chem.* **2005**, *53* (13), 5192−5199.

(8) Fujimoto, K.; Matsuda, K.; Aso, K. Acetolysis of polysaccharides III Preparation of laminaribiose from pachyman and laminarin by acetolysis. *Tohoku J. Agric. Res.* **1962**, *13*, 55−59.

(9) Takasuka, T. E.; Kim, H.; Deng, K.; Bianchetti, C. M.; Yamashita, K.; Beebe, E. T.; Bergeman, L. F.; Vander Meulen, K. A.; Deutsch, S.; Ralph, J.; Adams, P. D.; Northen, T. R.; Fox, B. G. Quantitative analysis of the high-yield hydrolysis of kelp by laminarinase and alginate lyase. *Chembiochem: a European journal of chemical biology* **2023**, *24* (20), No. e202300357.

(10) Jamois, F.; Goffic, F. L.; Yvin, J. C.; Plusquellec, D.; Ferrieres, V. How to improve chemical synthesis of laminaribiose on a large scale. *Open Glycosci.* **2008**, *1*, 19−24.

(11) Yvin, J.-C.; Jamios, F.; Ferrieres, V.; Plusquellec, D. Method for laminaribiose synthesis. U.S. Patent 6,632,940 B1, 2003, 2003.

(12) Kitaoka, M.; Matsuoka, Y.; Mori, K.; Nishimoto, M.; Hayashi, K. Characterization of a bacterial laminaribiose phosphorylase. *Biosci. Biotechnol. Biochem.* **2012**, *76* (2), 343−348.

(13) Zhang, Y. H. P.; Myung, S.; You, C.; Zhu, Z. G.; Rollin, J. A. Toward low-cost biomanufacturing through in vitro synthetic biology: bottom-up design. *J. Mater. Chem.* **2011**, *21* (47), 18877−18886.

(14) Niu, K. L.; Liu, Z. Y.; Feng, Y. H.; Gao, T. L.; Wang, Z. Z.; Zhang, P. P.; Du, Z. Q.; Gao, D. M.; Fang, X. A novel strategy for efficient disaccharides synthesis from glucose by β-glucosidase. *Bioresour Bioprocess* **2020**, *7* (1), 45−49.

(15) Xiao, Y.; Dong, S.; Liu, Y. J.; You, C.; Feng, Y.; Cui, Q. Key roles of β-glucosidase BglA for the catabolism of both laminaribiose and cellobiose in the lignocellulolytic bacterium Clostridium thermocellum. *Int. J. Biol. Macromol.* **2023**, *250*, 126226−126235.

(16) Nihira, T.; Saito, Y.; Kitaoka, M.; Nishimoto, M.; Otsubo, K.; Nakai, H. Characterization of a laminaribiose phosphorylase from Acholeplasma laidlawii PG-8A and production of 1,3-β-d-glucosyl disaccharides. *Carbohydr. Res.* **2012**, *361*, 49−54.

(17) Wang, L.; Zheng, P.; Hu, M.; Tao, Y. Inorganic phosphate self-sufficient whole-cell biocatalysts containing two co-expressed phosphorylases facilitate cellobiose production. *J. Ind. Microbiol. Biotechnol.* **2022**, *49* (3), kuac008.

(18) Du, Z. Q.; Li, F. Y.; Liu, Z. Y.; Tan, Y. S.; Niu, K. L.; Fang, X. Driving an in vitro multienzymatic cascade of laminaribiose biosynthesis from non-food cellulose with balancing the precursor supply. *Ind. Crops Prod.* **2022**, *182*, 114878−114885.

(19) You, C.; Chen, H.; Myung, S.; Sathitsuksanoh, N.; Ma, H.; Zhang, X. Z.; Li, J.; Zhang, Y. H. Enzymatic transformation of nonfood biomass to starch. *Proc. Natl. Acad. Sci. U.S.A.* **2013**, *110* (18), 7182−7187.

(20) Muller, C.; Hartig, D.; Vorlander, K.; Sass, A. C.; Scholl, S.; Jordening, H. J. Chitosan-based hybrid immobilization in bienzymatic reactions and its application to the production of laminaribiose. *Bioprocess Biosyst. Eng.* **2017**, *40* (9), 1399−1410.

(21) Sun, S.; Wei, X.; Zhou, X.; You, C. Construction of an artificial in vitro synthetic enzymatic platform for upgrading low-cost starch to value-added disaccharides. *J. Agric. Food Chem.* **2021**, *69* (1), 302−314.

(22) Sun, S.; You, C. Disaccharide phosphorylases: Structure, catalytic mechanisms and directed evolution. *Synth. Syst. Biotechnol.* **2021**, *6* (1), 23−31.

(23) You, C.; Shi, T.; Li, Y.; Han, P.; Zhou, X.; Zhang, Y. P. An in vitro synthetic biology platform for the industrial biomanufacturing of myo-inositol from starch. *Biotechnol. Bioeng.* **2017**, *114* (8), 1855−1864.

(24) Yuan, J. M.; Chyan, C. L.; Zhou, H. X.; Chung, T. Y.; Peng, H.; Ping, G.; Yang, G. The effects of macromolecular crowding on the mechanical stability of protein molecules. *Protein Sci.* **2008**, *17* (12), 2156−2166.

(25) Kuhaudomlarp, S.; Stevenson, C. E. M.; Lawson, D. M.; Field, R. A. The structure of a GH149 β-(1 → 3) glucan phosphorylase reveals a new surface oligosaccharide binding site and additional domains that are absent in the disaccharide-specific GH94 glucose-β-(1 → 3)-glucose (laminaribiose) phosphorylase. *Proteins* **2019**, *87* (10), 885−892.

(26) Kuhaudomlarp, S.; Pergolizzi, G.; Patron, N. J.; Henrissat, B.; Field, R. A. Unraveling the subtleties of β-(1→3)-glucan phosphorylase specificity in the GH94, GH149, and GH161 glycoside hydrolase families. *J. Biol. Chem.* **2019**, *294* (16), 6483−6493.

(27) Kuhaudomlarp, S.; Walpole, S.; Stevenson, C. E. M.; Nepogodiev, S. A.; Lawson, D. M.; Angulo, J.; Field, R. A. Unravelling the specificity of laminaribiose phosphorylase from Paenibacillus sp. YM-1 towards donor substrates glucose/mannose 1-phosphate by using x-ray crystallography and saturation transfer difference NMR spectroscopy. *Chembiochem: a European journal of chemical biology* **2019**, *20* (2), 181−192.

(28) Muller, C.; Ortmann, T.; Abi, A.; Hartig, D.; Scholl, S.; Jordening, H. J. Immobilization and characterization of E. Gracilis extract with enriched laminaribiose phosphorylase activity for bienzymatic production of laminaribiose. *Appl. Biochem. Biotechnol.* **2017**, *182* (1), 197−215.
(29) Marechal, L. R.; Goldemberg, S. H. Laminaribiose Phosphorylase from Euglena Gracilis. *Biochem. Bioph. Res. Co.* **1963**, *13* (2), 106−109.
(30) Kuhaudomlarp, S. The new families of β-(1−3)-glucan phosphorylases: identification, mechanisms and applications in carbohydrate synthesis. Doctoral Thesis, University of East Anglia, 2018.
(31) Kaur, J.; Sharma, R. Directed evolution: an approach to engineer enzymes. *Crit. Rev. Biotechnol.* **2006**, *26* (3), 165−199.
(32) Chen, R. Enzyme engineering: rational redesign versus directed evolution. *Trends Biotechnol.* **2001**, *19* (1), 13−14.
(33) Cherry, J. R.; Fidantsef, A. L. Directed evolution of industrial enzymes: an update. *Curr. Opin. Biotechnol.* **2003**, *14* (4), 438−443.
(34) Bloom, J. D.; Arnold, F. H. In the light of directed evolution: pathways of adaptive protein evolution. *Proc. Natl. Acad. Sci. U.S.A.* **2009**, *106* (supplement_1), 9995−10000.
(35) Zeldovich, K. B.; Chen, P.; Shakhnovich, E. I. Protein stability imposes limits on organism complexity and speed of molecular evolution. *Proc. Natl. Acad. Sci. U.S.A.* **2007**, *104* (41), 16152−16157.
(36) Banga, J. R. Optimization in computational systems biology. *BMC Syst. Biol.* **2008**, *2* (1), 47−53.
(37) Jaenicke, R.; Schurig, H.; Beaucamp, N.; Ostendorp, R. Structure and stability of hyperstable proteins: glycolytic enzymes from hyperthermophilic bacterium Thermotoga maritima. *Adv. Protein Chem.* **1996**, *48*, 181−269.
(38) Lehmann, M.; Kostrewa, D.; Wyss, M.; Brugger, R.; D'Arcy, A.; Pasamontes, L.; van Loon, A. P. From DNA sequence to improved functionality: using protein sequence comparisons to rapidly design a thermostable consensus phytase. *Protein Eng.* **2000**, *13* (1), 49−57.
(39) Borgo, B.; Havranek, J. J. Automated selection of stabilizing mutations in designed and natural proteins. *Proc. Natl. Acad. Sci. U.S.A.* **2012**, *109* (5), 1494−1499.
(40) Cui, Y. L.; Sun, J. Y.; Wu, B. Computational enzyme redesign: large jumps in function. *Trends Chem.* **2022**, *4* (5), 409−419.
(41) Wijma, H. J.; Furst, M.; Janssen, D. B. A computational library design protocol for rapid improvement of protein stability: FRESCO. *Methods Mol. Biol.* **2018**, *1685*, 69−85.
(42) Bednar, D.; Beerens, K.; Sebestova, E.; Bendl, J.; Khare, S.; Chaloupkova, R.; Prokop, Z.; Brezovsky, J.; Baker, D.; Damborsky, J. FireProt: Energy- and evolution-based computational design of thermostable multiple-point mutants. *PLoS Comput. Biol.* **2015**, *11* (11), No. e1004556.
(43) Goldenzweig, A.; Goldsmith, M.; Hill, S. E.; Gertman, O.; Laurino, P.; Ashani, Y.; Dym, O.; Unger, T.; Albeck, S.; Prilusky, J.; Lieberman, R. L.; Aharoni, A.; Silman, I.; Sussman, J. L.; Tawfik, D. S.; Fleishman, S. J. Automated structure- and sequence-based design of proteins for high bacterial expression and stability. *Mol. Cell* **2016**, *63* (2), 337−346.
(44) Cui, Y. L.; Chen, Y. C.; Liu, X. Y.; Dong, S. J.; Tian, Y. E.; Qiao, Y. X.; Mitra, R.; Han, J.; Li, C. L.; Han, X.; Liu, W. D.; Chen, Q.; Wei, W. Q.; Wang, X.; Du, W. B.; Tang, S. Y.; Xiang, H.; Liu, H. Y.; Liang, Y.; Houk, K. N.; Wu, B. Computational redesign of a PETase for plastic biodegradation under ambient condition by the GRAPE strategy. *ACS Catal.* **2021**, *11* (3), 1340−1350.
(45) Hopf, T. A.; Green, A. G.; Schubert, B.; Mersmann, S.; Scharfe, C. P. I.; Ingraham, J. B.; Toth-Petroczy, A.; Brock, K.; Riesselman, A. J.; Palmedo, P.; Kang, C.; Sheridan, R.; Draizen, E. J.; Dallago, C.; Sander, C.; Marks, D. S. The EVcouplings Python framework for coevolutionary sequence analysis. *Bioinformatics* **2019**, *35* (9), 1582−1584.
(46) Anishchenko, I.; Ovchinnikov, S.; Kamisetty, H.; Baker, D. Origins of coevolution between residues distant in protein 3D structures. *Proc. Natl. Acad. Sci. U.S.A.* **2017**, *114* (34), 9122−9127.
(47) Buß, O.; Rudat, J.; Ochsenreither, K. FoldX as protein engineering tool: Better than random based approaches? *Comput. Struct. Biotechnol. J.* **2018**, *16*, 25−33.
(48) Liu, Y.; Kuhlman, B. RosettaDesign server for protein design. *Nucleic Acids Res.* **2006**, *34*, W235−W238.
(49) Craig, D. B.; Dombkowski, A. A. Disulfide by Design 2.0: a web-based tool for disulfide engineering in proteins. *BMC Bioinf.* **2013**, *14*, 346−351.
(50) Tanford, C.; Kirkwood, J. G. Theory of protein titration curves. I. General equations for impenetrable spheres. *J. Am. Chem. Soc.* **1957**, *79* (20), 5333−5339.
(51) Richmond, T. J. Solvent accessible surface area and excluded volume in proteins. *J. Mol. Biol.* **1984**, *178* (1), 63−89.
(52) Bashford, D.; Karplus, M. Multiple-site titration curves of proteins: an analysis of exact and approximate methods for their calculation. *J. Phys. Chem. B* **1991**, *95* (23), 9556−9561.
(53) Havranek, J. J.; Harbury, P. B. Tanford-Kirkwood electrostatics for protein modeling. *Proc. Natl. Acad. Sci. U.S.A.* **1999**, *96* (20), 11145−11150.
(54) You, S.; Tu, T.; Zhang, L.; Wang, Y.; Huang, H.; Ma, R.; Shi, P.; Bai, Y.; Su, X.; Lin, Z.; Luo, H.; Yao, B. Improvement of the thermostability and catalytic efficiency of a highly active β-glucanase from Talaromyces leycettanus JCM12802 by optimizing residual charge−charge interactions. *Biotechnol. Biofuels* **2016**, *9*, 124−135.
(55) Zhang, L.; Tang, X.; Cui, D.; Yao, Z.; Gao, B.; Jiang, S.; Yin, B.; Yuan, Y. A.; Wei, D. A method to rationally increase protein stability based on the charge-charge interaction, with application to lipase LipK107. *Protein Sci.* **2014**, *23* (1), 110−116.
(56) Van Der Spoel, D.; Lindahl, E.; Hess, B.; Groenhof, G.; Mark, A. E.; Berendsen, H. J. GROMACS: fast, flexible, and free. *J. Comput. Chem.* **2005**, *26* (16), 1701−1718.
(57) Sun, Z.; Liu, Q.; Qu, G.; Feng, Y.; Reetz, M. T. Utility of B-factors in protein science: Interpreting rigidity, flexibility, and internal motion and engineering thermostability. *Chem. Rev.* **2019**, *119* (3), 1626−1665.
(58) Jumper, J.; Evans, R.; Pritzel, A.; Green, T.; Figurnov, M.; Ronneberger, O.; Tunyasuvunakool, K.; Bates, R.; Zidek, A.; Potapenko, A.; Bridgland, A.; Meyer, C.; Kohl, S. A. A.; Ballard, A. J.; Cowie, A.; Romera-Paredes, B.; Nikolov, S.; Jain, R.; Adler, J.; Back, T.; Petersen, S.; Reiman, D.; Clancy, E.; Zielinski, M.; Steinegger, M.; Pacholska, M.; Berghammer, T.; Bodenstein, S.; Silver, D.; Vinyals, O.; Senior, A. W.; Kavukcuoglu, K.; Kohli, P.; Hassabis, D. Highly accurate protein structure prediction with AlphaFold. *Nature* **2021**, *596* (7873), 583−589.
(59) Varadi, M.; Anyango, S.; Deshpande, M.; Nair, S.; Natassia, C.; Yordanova, G.; Yuan, D.; Stroe, O.; Wood, G.; Laydon, A.; Zidek, A.; Green, T.; Tunyasuvunakool, K.; Petersen, S.; Jumper, J.; Clancy, E.; Green, R.; Vora, A.; Lutfi, M.; Figurnov, M.; Cowie, A.; Hobbs, N.; Kohli, P.; Kleywegt, G.; Birney, E.; Hassabis, D.; Velankar, S. AlphaFold Protein Structure Database: massively expanding the structural coverage of protein-sequence space with high-accuracy models. *Nucleic Acids Res.* **2022**, *50* (D1), D439−D444.
(60) Ellman, G. L. Tissue sulfhydryl groups. *Arch. Biochem. Biophys.* **1959**, *82* (1), 70−77.
(61) You, C.; Huang, Q.; Xue, H.; Xu, Y.; Lu, H. Potential hydrophobic interaction between two cysteines in interior hydrophobic region improves thermostability of a family 11 xylanase from Neocallimastix patriciarum. *Biotechnol. Bioeng.* **2010**, *105* (5), 861−870.
(62) Tanner, D. E.; Chan, K. Y.; Phillips, J. C.; Schulten, K. Parallel generalized born implicit solvent calculations with NAMD. *J. Chem. Theory Comput.* **2011**, *7* (11), 3635−3642.
(63) Hess, B.; Bekker, H.; Berendsen, H. J. C.; Fraaije, J. G. E. M. LINCS: A linear constraint solver for molecular simulations. *J. Comput. Chem.* **1997**, *18* (12), 1463−1472.
(64) Li, Y.; Liu, S.; You, C. Permeabilized escherichia coli whole cells containing co-expressed two thermophilic enzymes facilitate the synthesis of scyllo-Inositol from myo-Inositol. *Biotechnol. J.* **2020**, *15* (2), No. e1900191.

https://doi.org/10.1021/acssuschemeng.3c06089
ACS Sustainable Chem. Eng. XXXX, XXX, XXX−XXX

(65) Ban, X.; Wu, J.; Kaustubh, B.; Lahiri, P.; Dhoble, A. S.; Gu, Z.; Li, C.; Cheng, L.; Hong, Y.; Tong, Y.; Li, Z. Additional salt bridges improve the thermostability of 1,4-α-glucan branching enzyme. *Food Chem.* **2020**, *316*, 126348−126355.
(66) Cui, H.; Eltoukhy, L.; Zhang, L.; Markel, U.; Jaeger, K. E.; Davari, M. D.; Schwaneberg, U. Less unfavorable salt bridges on the enzyme surface result in more organic cosolvent resistance. *Angew. Chem., Int. Ed. Engl.* **2021**, *60* (20), 11448−11456.
(67) Hopf, T. A.; Scharfe, C. P.; Rodrigues, J. P.; Green, A. G.; Kohlbacher, O.; Sander, C.; Bonvin, A. M.; Marks, D. S. Sequence co-evolution gives 3D contacts and structures of protein complexes. *eLife* **2014**, *3*, No. e03430.
(68) Zhang, L.; Yin, B.; Wang, C.; Jiang, S.; Wang, H.; Yuan, Y. A.; Wei, D. Structural insights into enzymatic activity and substrate specificity determination by a single amino acid in nitrilase from Syechocystis sp. PCC6803. *J. Struct. Biol.* **2014**, *188* (2), 93−101.
(69) Yang, Y.; Zhang, L.; Guo, M.; Sun, J.; Matsukawa, S.; Xie, J.; Wei, D. Novel alpha-L-arabinofuranosidase from Cellulomonas fimi ATCC 484 and its substrate-specificity analysis with the aid of computer. *J. Agric. Food Chem.* **2015**, *63* (14), 3725−3733.
(70) Tu, T.; Luo, H.; Meng, K.; Cheng, Y.; Ma, R.; Shi, P.; Huang, H.; Bai, Y.; Wang, Y.; Zhang, L.; Yao, B. Improvement in thermostability of an Achaetomium sp. Strain Xz8 endopolygalacturonase via the optimization of charge-charge interactions. *Appl. Environ. Microbiol.* **2015**, *81* (19), 6938−6944.
(71) Jiang, S.; Zhang, L.; Cui, D.; Yao, Z.; Gao, B.; Lin, J.; Wei, D. The important role of halogen bond in substrate selectivity of enzymatic catalysis. *Sci. Rep.* **2016**, *6*, 34750−34756.
(72) Qu, G.; Bi, Y.; Liu, B.; Li, J.; Han, X.; Liu, W.; Jiang, Y.; Qin, Z.; Sun, Z. Unlocking the stereoselectivity and substrate acceptance of enzymes: Proline-induced loop engineering test. *Angew. Chem., Int. Ed. Engl.* **2022**, *61* (1), No. e202110793.
(73) Ye, X.; Zhang, C.; Zhang, Y. H. Engineering a large protein by combined rational and random approaches: stabilizing the Clostridium thermocellum cellobiose phosphorylase. *Mol. Biosyst.* **2012**, *8* (6), 1815−1823.
(74) Kumar, S.; Seth, D.; Deshpande, P. A. Molecular dynamics simulations identify the regions of compromised thermostability in SazCA. *Proteins* **2021**, *89* (4), 375−388.
(75) Chakrabarti, P.; Chakrabarti, S. C—H···O hydrogen bond involving proline residues in α-helices. *J. Mol. Biol.* **1998**, *284* (4), 867−873.
(76) Rios, N. S.; Pinheiro, M. P.; dos Santos, J. C. S.; de S Fonseca, T.; Lima, L. D.; de Mattos, M. C.; Freire, D. M. G.; da Silva, I. J.; Rodríguez-Aguado, E.; Gonçalves, L. R. Strategies of covalent immobilization of a recombinant Candida antarctica lipase B on pore-expanded SBA-15 and its application in the kinetic resolution of (R , S)-Phenylethyl acetate. *J. Mol. Catal. B-Enzym.* **2016**, *133*, 246−258.
(77) Bepler, T.; Berger, B. Learning the protein language: Evolution, structure, and function. *Cell Syst.* **2021**, *12* (6), 654−669.e3.
(78) Gao, X.; Dong, X.; Li, X.; Liu, Z.; Liu, H. Prediction of disulfide bond engineering sites using a machine learning method. *Sci. Rep.* **2020**, *10* (1), 10330−10338.
(79) Liu, M.; Song, Y.; Zhang, Y. P. J.; You, C. Carrier-free immobilization of multi-enzyme complex facilitates in vitro synthetic enzymatic biosystem for biomanufacturing. *ChemSusChem* **2023**, *16* (6), No. e202202153.

https://doi.org/10.1021/acssuschemeng.3c06089
ACS Sustainable Chem. Eng. XXXX, XXX, XXX−XXX